International Atomic Energy Agency

INDC(AUL)-032/G

INDC INTERNATIONAL NUCLEAR DATA COMMITTEE

PROGRESS REPORT

ON

NUCLEAR DATA ACTIVITIES IN AUSTRALIA FOR 1983-1984

compiled by

J.W. Boldeman

Australian Atomic Energy Commission Research Establishment
Lucas Heights Research Laboratories
Private Mail Bag, Sutherland, NSW 2232, Australia

September 1984

IAEA NUCLEAR DATA SECTION, WAGRAMERSTRASSE 5, A-1400 VIENNA

INDC(AUL)-032/G

Progress Report

on

Nuclear Data Activities in Australia for 1983-1984

compiled by

J.W. Boldeman

Australian Atomic Energy Commission Research Establishment
Lucas Heights Research Laboratories
Private Mail Bag, Sutherland, NSW 2232, Australia

September, 1984

CONTENTS

1. AUSTRALIAN ATOMIC ENERGY COMMISSION

1.1 Fission Neutron Spectrum from the Spontaneous Fission of ^{252}Cf (Boldeman)

The fission neutron spectrum from the spontaneous fission of ^{252}Cf has been measured in the energy range, 0.124 to 15.0 MeV, using the time-of-flight method. Seven separate measurements covering the energy range, 1 to 15 MeV, were performed with an NE102 plastic scintillator. Preliminary data from the first six of these measurements have been reported [1,2]. For the energy range, 0.124 to 2.6 MeV a ^{6}Li enriched glass scintillator was used. The data have been finalised and a paper describing the measurements and outlining all sources of error has been submitted to Nuclear Science and Engineering.

It has been found that the spectrum can be represented fairly accurately by a Maxwellian distribution, $N(E)=A\ E^{\frac{1}{2}} \exp(-E/T)$ in which the experimental value for the average energy, $\bar{E}=3T/2$, is 2.136 ± 0.019 MeV. In the energy range 0.8-15.0 MeV, the experimental data are consistent within the experimental accuracy with the Maxwellian shape. Figure 1 shows the experimental data between 1 and 15 MeV for experiment 7 and the fitted Maxwellian distribution. The data from the ^{6}Li experiment are shown in Figure 2 together with the Maxwellian distribution normalised between 0.95 and 1.35 MeV. For the data below 0.8 MeV, there is evidence for a negative deviation of the order of 5% between 0.4 and 0.8 MeV.

References

1. J.W. Boldeman, D. Culley and R.J. Cawley (1978)
   Proc. Int. Conf. on Neutron Physics and Nuclear Data, Harwell, p 916.
2. J.W. Boldeman, D. Culley and R.J. Cawley (1979)
   ANS Trans. 32, 733.

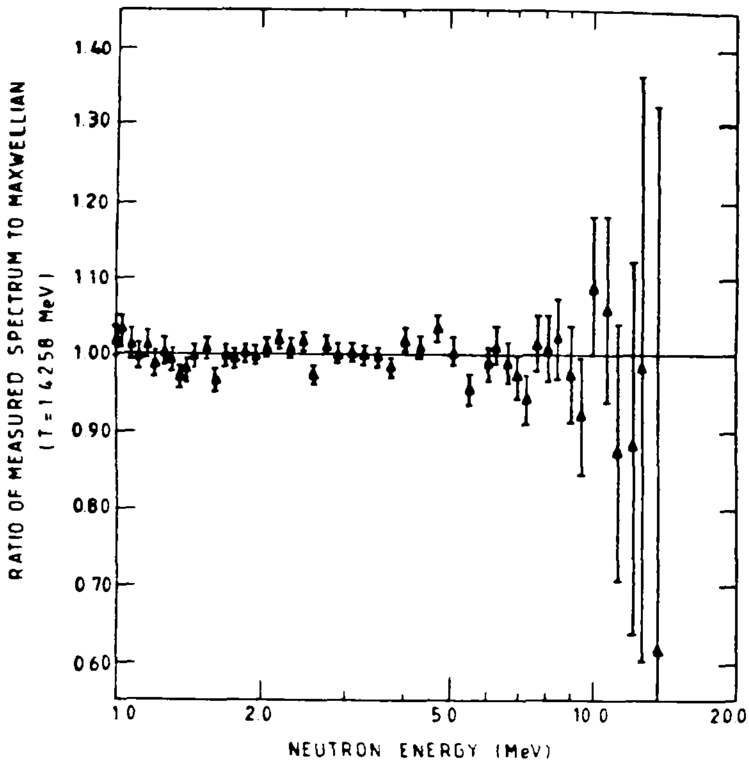

Figure 1 Experimental data from Experiment 7 compared with fitted Maxwellian distribution. (At lower energy end of the curve, every second point only is plotted)

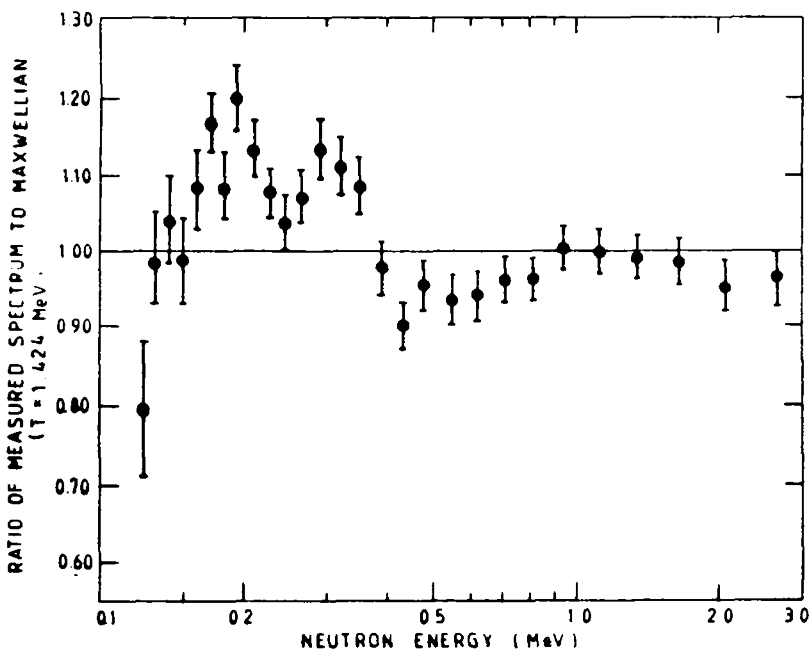

Figure 2 Experimental data from the measurement with the ^{6}Li glass scintillator

1.2 Prompt Neutron Emission Parameters (Boldeman, Hines)

There has been renewed interest in the neutron emission probability distributions following spontaneous and thermal neutron-induced fission because of the relevance of such data in neutron coincidence counting systems. The experimental data for neutron fission of ^{233}U, ^{235}U, ^{239}Pu and ^{241}Pu and for spontaneous fission of ^{240}Pu, ^{242}Pu and ^{252}Cf previously reported have been revised and extended by some unpublished data. A paper listing the new data has been submitted to Nuclear Science and Engineering.

1.3 The Fission Barrier for ^{230}Th (Boldeman, Walsh)

Fission fragment angular distributions for neutron fission of ^{230}Th in the energy range 680-1100 MeV have been published sometime ago.[1] These data together with similar fission fragment angular distribution studies an the measured fission neutron cross section of ^{230}Th from Blons et al [2] were interpreted in terms of a vibrational resonance in the third well of a triple-humped fission barrier. In the analysis two rotational bands with the same intrinsic spin (K=1/2) but opposite parity were required to fit the data. A further feature in the analysis was the requirement of opposite signs for the decoupling parameters for the two parity bands.

The question of a triple-humped shape for the fission barriers of the Thorium nuclei has been a controversial subject for some time, (ref 3 and discussion), and all analyses of the data have been subject to some criticism, [e.g. see ref 4)]. With reference to our previous studies, the criticism has been based on some differences between our experimental angular distributions and those from other experiments [data in ref 1) and refs 5) & 6)]. Furthermore some doubts have been expressed regarding the energy resolution. The experiments were performed with energy resolutions (full width) of either 8 or 16 MeV.

Because of these criticisms the experiments have been repeated. The energy calibration of the 3 MV Van de Graaff accelerator has been based on resonances in ^{32}S, ^{9}Be, ^{16}O and ^{28}Si. The energy resolution has been determined experimentally for each measurement by measuring the total cross section of ^{32}S for the two resonances at 724.8 keV and 740 keV. The data previously published have been confirmed and are being extended. The fission barrier parameters presented in ref 1) still provide the best fit to all the experimental data.

References

1) J.W. Boldeman, D. Gogny, A.R. del Musgrove and R.L.Walsh (1980), Phys. Rev. 22 , 627.

2) J. Blons, C. Mazur, D. Paya, M. Ribrag and H. Weigmann (1978), Phys. Rev. Lett. 41, 1282.

3) D. Paya (1979) Procs. IAEA Symposium on Physics and Chemistry of Fission, Julich (1979), Vol. 1, page 207.

4) S. Björnholm and J.E. Lynn (1980) Rev. of Mod. Phys. 52, 725.

5) D.W. Muir and L.R. Veeser (1981) Phys. Rev. 24, 1540.

6) G.D. James, D.B. Syme and J. Grainger (1983), 205, 151.

1.4 On The Effect Of Scission Neutrons On $\nu(A)$ Data For $^{252}Cf(s\ f)$ (Walsh and Boldeman)

In measurements of $\nu(A)$, the neutron emission from individual fragments, the scission neutron proportion enters via the correction that is applied to the measured data on account of the neutron detection geometry. The scission neutrons are assumed to be emitted isotropically in the centre of mass system (CMS) of the compound nucleus, while the 'fragment' neutrons are emitted in the CMS of the fragment and are thus peaked in the fragment forward direction.

It is of interest to determine the variation of $\nu(A)$ data as a function of this scission neutron proportion. The interest is both inherent in the problem and also because the $\nu(A)$ shape itself can be used as a check on the adequacy of calculations of the neutron energy spectrum (Madland and Nix[1]). We have re-analysed our $\nu(A)$ data for $^{252}Cf(s\ f)$ [Ref. 2] to examine the effects of various assumed scission neutron proportions. In Ref. 2 a scission neutron proportion of 15% was used and the scission neutron were assumed to have an energy spectrum similar to that of the fragment neutrons.

The scission neutron proportions FSIS assumed were 0, 5, 10, 15, 20 and 25%. Figure 1 shows the results for FSIS=0, 10 and 20%. For an FSIS change from 0-20%, $\nu(A)$ increases by 5.3% at A = 124 amu and decreases by some 5.0% at 130 amu. The changes are less at the $\nu(A)$ outer extremes, viz a decrease of 3.4% at 90 amu and an increase of 0.6% at 160 amu. The changes in sign of the correction to $\nu(A)$ as A increases across the $\nu(A)$ curve are to be expected, from the nature of the neutron geometry correction[3].

Figure 1 also shows the results for $\nu_{TOT}(A)$, the neutron emission from two complementary fragments. The changes in $\nu_{TOT}(A)$ are uniformly less for $\nu(A)$. For an FSIS change from 0-20%, $\Delta\nu_{TOT}(A)$ equals -2.3% at 130 amu, + 0.6% at 148 amu and -0.5% at 160 amu. $\Delta\nu_{TOT}(A)$ has its maximum value of -2.9% at symmetric fission.

---

* To be published in Journal of Nuclear Science and Engineering.

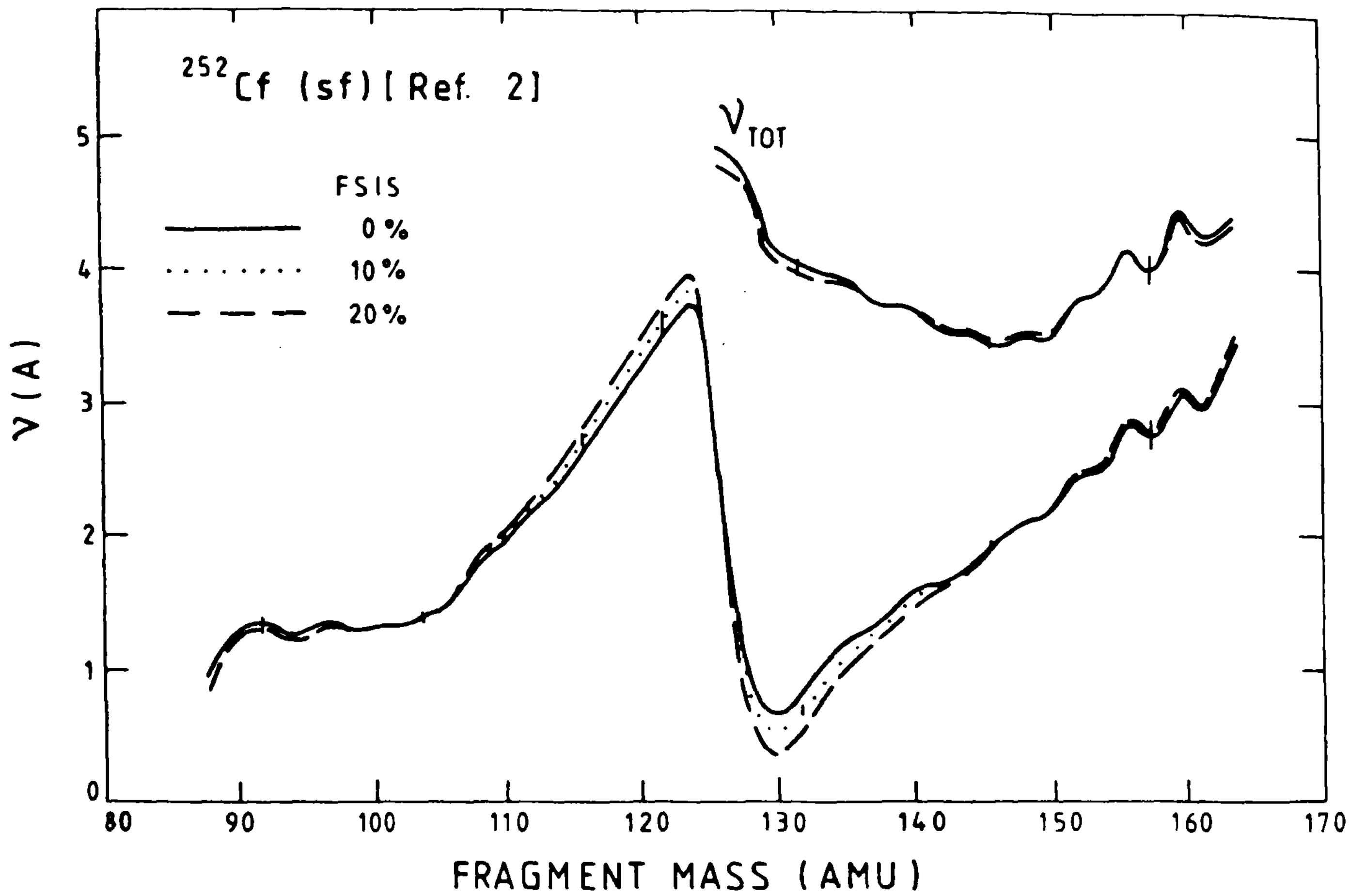

FIGURE 1 ν(A) RESULTS FOR VARIOUS ASSUMED SCISSION NEUTRON PROPORTIONS FSIS.
—— FSIS = 0%, ... FSIS = 10%, – – – – FSIS = 20%.
SOME DATA ERROR BARS ARE SHOWN, FOR FSIS = 10% CURVE.

References

1) Madland, D.G. and Nix, J.R. - Int. Conf. on Nuclear Data, Antwerp 1982, p.473.

2) Walsh, R.L. and Boldeman, J.W. - Nucl. Phys. A276 (1977) 189.

3) Boldeman, J.W., Musgrove, A.R. de L. and Walsh, R.L. - Aust. J. Phys. 24 (1971) 821.

1.5 Variation Of Even-Odd Effects In $\nu(A)$ With Excitation Energy (Walsh)

The variation with excitation energy of fine structure reported [1] in $\nu(A)$ for $^{252}Cf(sf)$ has been examined. The method is to set windows on the $\nu(A)$ and $Y(A)$ data which are parallel to the contour lines in the E_L vs mass surface. This procedure is similar to that used by Fraser, Milton et al [2] to highlight their $^{252}Cf(sf)$ $Y(A)$ fine structure. The window radii are varied from 9 to 25 MeV. Thus the procedure examines how the $\nu(A)$ and $Y(A)$ fine structure vary simultaneously as the total excitation energy E^* decreases.

The results show that the $Y(A)$ fine structure becomes more prominent as E^* decreases, a phenomenon which is well known [3]. Also, the amplitude of the $\nu(A)$ fine structure increases as E^* decreases. This occurs for each of ν_L, ν_H, and ν_{TOT}. Further the structure consistently occurs at the expected mass locations [4]. This variation confirms that the fine structure in $\nu(A)$ data is related to even-odd Z effects.

The increase in amplitude of the $\nu(A)$ fine structure is also apparent when linear windows of E_L = constant are applied to the data (Figures 1 and 2).

The trend with excitation energy observed in this work appears to be at variance with the 'cold fission' data of ref.[5] which found no even-odd Z effects at very low excitation energy for ^{233}, $^{235}U(n,f)$.

References

1) R.L. Walsh and J.W. Boldeman, Nucl. Phys. A276 (1977) 189.

2) J.S. Fraser, J.C.D. Milton et al., Can. J. Phys. 41 (1963) 2080.

3) W.N. Reisdorf, U.P. Unik and L.E. Glendenin, Nucl. Phys. A205 (1973) 348.

4) J.P. Unik, J.E. Gindler et al., 3rd IAEA Symp. Phys. and Chem. of Fission, Rochester, 1973, Vol. 2, p 19.

5) C. Signarbieux, M. Montova et al., J. Physique - Lettres 42 (1981) L-437.

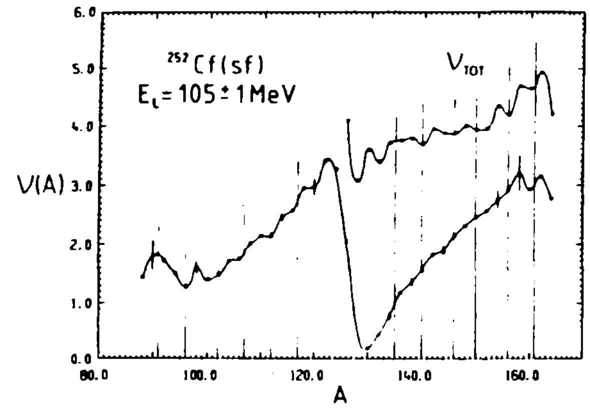

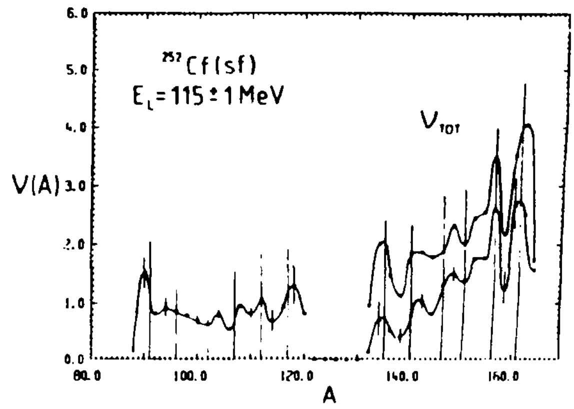

Fig. 1 ν(A) results for E_L = 105 1 MeV. Vertical lines show locations of A_L and A_H for evenly charged fragments[4]

Fig. 2 ν(A) results for E_L = 115 ± 1 MeV.

1.6 The Mass Resolution Correction in Double-Energy Fission Measurements (Lang, Walsh)

The limitations of mass resolution in double-energy fission fragment measurements have been examined. The measured mass yield curves were then corrected for mass resolution by two methods:

(i) Five-element operator method

The measured yield at a given mass is a linear combination of the source spectrum over some range of masses. One calculates the inverse of the linear operator to recover the source spectrum as a linear combination of the measured mass yields for some selection of neighbouring points.

(ii) Iterative Method

The essence of an interative method can be seen by following one cycle of iterations. The approximate form of the spectrum generated in the previous cycle is folded with the known resolution function to produce a set of predicted yields. The predicted yields are compared with the measured yields and the discrepancies are used to generate a corrected form of the spectrum for use at the next iteration. Figure 1 shows the results obtained after five iterations for the ^{239}Pu (n,f) data of |1|. The operator method gives similar results.

1.7 Evidence for Valence Transitions in Neutron Capture Gamma-Ray Spectra in ^{88}Sr (Allen, Company*)

Neutron capture γ-ray spectra have been measured at 11 average neutron energies from 10 to 530 keV in ^{88}Sr using a 20 x 15 cm NaI detector with time-of-flight discrimination of background events. The partial radiation widths and the calculated partial valence widths are compared for the strong p-wave resonances at 287 and 321 keV and found to be highly correlated. At these energies, the spectra are dominated by strong transitions to low-lying single particle states, in confirmation of the role of valence capture in the 3p region. However, the data do not support this mechanism at <508> keV.

1.8 Gamma-Ray Strength Functions in ^{139}La and ^{141}Pr (Allen, Company)

Neutron capture γ-ray spectra at average neutron energies <180> and <270> keV in ^{139}La and at <35>, <270>, <725> and <1075> keV in ^{141}Pr have been measured with a NaI detector. The corrected energy level distributions are obtained and γ-ray strength functions investigated. The data fit well within the framework of the Lorentzian giant dipole resonance. The non-statistical capture mechanism hypothesis is ruled out as a dominant capture mechanism in these nuclides in the threshold region.

1.9 Valence Neutron Capture In s- and p-Wave Resonances in ^{32}S (Allen, Company)

Neutron capture γ-ray spectra from resonances with large reduced neutron widths have been measured in ^{32}S. Spectra were obtained with a large NaI detector with time-of-flight discrimination of resonance capture events. Partial radiation widths are deduced and found to be consistent with a major valence contribution in both the 102.7 keV s-wave and 202.6 keV p-wave resonances. The observed and calculated valence partial radiation widths are found to be highly correlated, supporting an important role for the valence model in both s- and p- wave resonances in ^{32}S.

---

* University of Wollongong

2. AUSTRALIAN INSTITUTE OF NUCLEAR SCIENCE AND ENGINEERING.

2.1 L Subshell X-ray Production by 1-3 MeV Protons and He^+ Ions (Cohen)

Individual L subshell ionisation cross sections for proton and He ion bombardment of selected heavy targets between Gd and U have been measured for the ion energy range 1-3 MeV [1]. The experimental results have been compared in detail with the latest ECPSSR theory of Brandt and Lapicki[2]. This theory is essentially the Plane Wave Born approximation corrected for relatistic effects of the target electrons (R), the perturbing effect of the ion on the stationary states of the target electrons (PSS), the Coulomb deflection effect of the target nucleus in the impinging ion (C), and finally the small energy loss effects (E) felt by the ion while travelling in the coulomb field of the target nucleus. The ECPSSR predictions are good for high ion velocities, however for low ion velocities large discrepancies occur for the L_2 subshell. This effect has been studied closely with a view to interpreting it in terms of either collision induced transitions between L subshells or a completely new approach to the individual subshell coulomb deflection factors. Figures 1 to 3 show the ratio of experiment to the ECPSSR theory, for the 3 L subshells, versus the reduced ion velocity.

These differences were found to be exponential in nature when plotted against the coulomb deflection parameter[2] $x_s=\left[2\pi d q_{os}\zeta\ /Z_s(1 + Z_s)\right]$. See figure 4. This enabled us to define new experimental subshell coulomb deflection factors $\exp\left[-\gamma_s \pi x_s\right]$ where γ_s is given in Table 1. Previously $\gamma_s = \gamma_B = 1.111$ for all three subshells in the Brandt and Lapicki theory[2].

TABLE 1

Shell	γ_s
L_1	$\gamma_1 = 0.952 \pm 0.19$
L_2	$\gamma_2 = 0.113 \pm 0.09$
L_3	$\gamma_3 = 0.811 \pm 0.10$
L_{TOTAL}	$\gamma_{TOTAL} = 0.824 \pm 0.11$

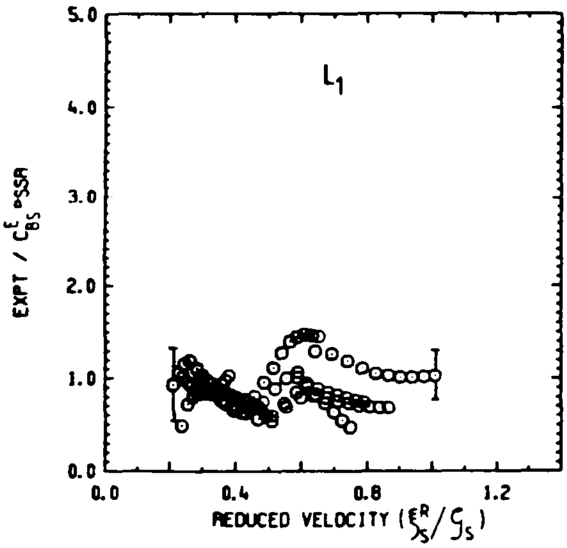

Fig. 1 A Comparison of the mean of the thin and thick experimental data with the ECPSSR theory as a function of the corrected reduced ion velocity for the L_1 subshell.

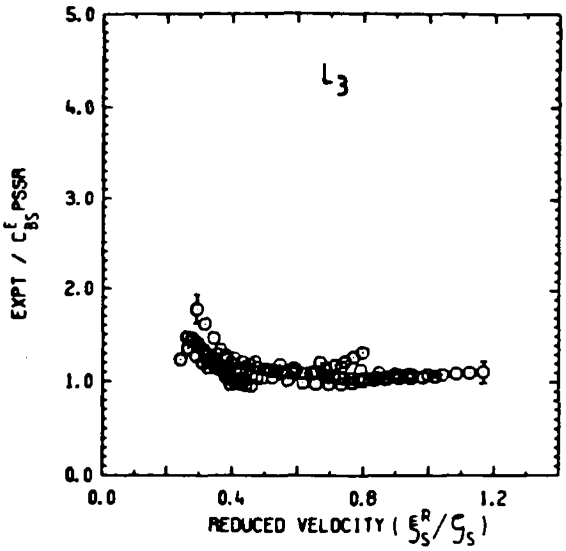

Fig. 3 As for Fig.1, for the L_3 subshell.

2.2 The $^{18}O(p,\alpha)^{15}N$ Reaction for ^{18}O Enriched Water In Small Biological Samples (Cohen°, Katsaros°, Bradshaw*, Garton+).

The discovery that the oxygen of respiratory CO_2 is in isotopic equilibrium with the oxygen of body water in animals paved the way for studies on the material and energy balance of free-ranging animals. Oxygen in the body is turned over as a result of exchange of both CO_2 and H_2O with the environment and, if the hydrogen turnover is known independently, then CO_2 production can be estimated. The advantage of this approach is that energy metabolism can be measured in unrestrained animals living normally in their natural habitat and it is evident that many of the accepted data on energy metabolism in animals, derived from laboratory experiments, are seriously in error.

Currently animals are injected with $^{3}HH^{18}O$ (ca. 3ml/kg of 97% enriched ^{18}O). ^{3}H turnover is then assessed by liquid scintillation counting and ^{18}O concentrations are analysed by the $^{18}O(p,n)^{18}F$ nuclear reaction at the UCLA Laboratory of Nuclear Medicine and Radiation Biology, using 22.1 MeV protons produced by a medical cyclotron. The disadvantages of this method

---

°AINSE; *Uni. of W.A.; +AAEC

are the high costs involved ($US 550/30 samples) and the inevitable delays associated with sending samples overseas for analysis and these constraints have motivated our development of an alternative method of analysis which utilises the $^{18}O(p,\alpha)^{15}N$ nuclear reaction in the 3MV Van de Graaff Accelerator at Lucas Heights.

To do this we have studied the broad resonance at a proton energy of 846 keV. The FWHM of the resonance was found to be (47±1)keV and the peak cross section in the centre of mass frame for a 90° centre of mass scattering angle was (41±6)mb. The normalised cross section versus proton energy is shown in Figure 1 for various scattering angles in the lab frame. The cross section was not isotopic and varied from σ_{cm} = (57±6)ub at θ_{cm} = 30° to (38±2)mb at θ_{cm} = 150°.

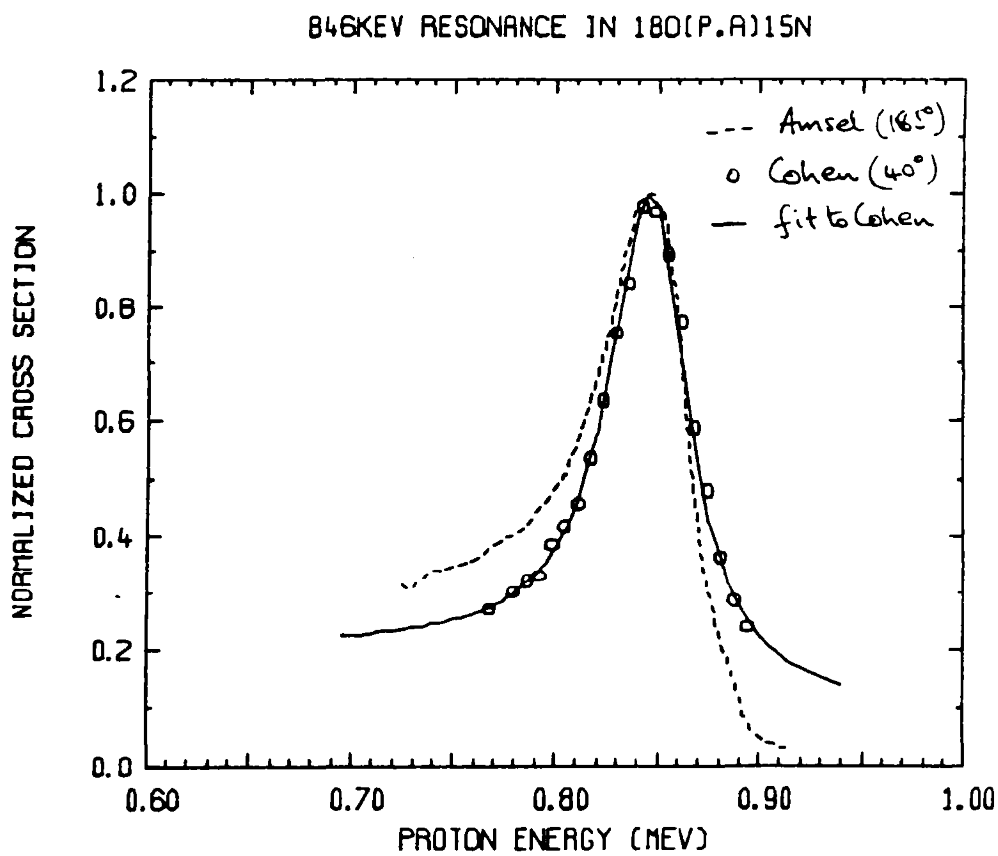

3. AUSTRALIAN NATIONAL UNIVERSITY

3.1 Introduction

The principal research facility of the Department of Nuclear Physics of the Australian National University is a 14UD Tandem Acceleration. There is in addition a 2 MeV Van de Graaff accelerator which is used for some calibration experiments and occasionally for some Applied Physics studies. The overall research program can be divided into a number of areas.

(i) Accelerator Development
(ii) Fission and Fusion Studies
(iii) Nuclei far from Stability
(iv) Nuclear Reactions and Scattering
(v) Coulomb Excitation
(vi) Discrete γ-ray Spectroscopy
(vii) Hyperfine Interactions
(viii) Atomic Collisions in Solids
(ix) Mass Spectroscopy

Most of these research activities are outside the scope of the present report and in these cases an overview only is given. Full details of the research programs can be obtained from Prof. J.O. Newton.

3.1.1 Operational Performance of the Super Buncher System (England, Stewart, Weisser, Leigh, Ophel)

Measurements have been made of the intrinsic beam bunch width and of the effective beam bunching efficiency of the split-loop resonator super buncher fed with pulses of about 700 picosec FWHM from the room temperature pulsing system. A beam of 62.5 MeV ^{12}C ions was scattered at 25° lab from thin gold targets and detected in silicon surface barrier detectors having average fields of approximately 1.6 volts micron^{-1}. These observations were performed at two distances from the centre of the super buncher, 5 m and 17 m. Tests were also carried out to determine the intrinsic time resolution of the silicon detectors used for the measurements.

The intrinsic time resolution of the electronics was 20 picosec FWHM for pulses of the type generated by the fast LeCroy discriminator units (Figure 1a). The time spectrum of a closely spaced silicon detector telescope using the same electronics and an 85 MeV beam of ^{19}F ions (which deposited equal amounts of energy in each detector) is shown in Figure 1b. The value of 72.8 picosec FWHM obtained implies an intrinsic time resolution for a single detector of 49.5 picosec FWHM. The time spectrum obtained at 5 m from the super buncher (Figure 1c) using a single detector and the bunched beam also yielded a value of 72.8 picosec FWHM, while the similar time spectrum taken at 17m from the super buncher (Figure 1d) gave a value of 89.7 picosec FWHM. Using the data shown, we unfold an intrinsic beam pulse width of 46.8 picosec FWHM and an energy spread entering the super buncher of 12.4 keV FWHM for the 62.5 MeV ^{12}C ion beam.

Measurements taken at the same time with the super buncher only in operation indicate a bunching efficiency for a d.c. beam of 29%. A two-dimensional plot of beam energy versus time taken in this mode is shown in Figure 2. Combining this result with the room temperature pulsing system, an overall bunching efficiency of approximately 20% of d.c. beam is obtained for the transmission of the pulsed beam through the full system for a 53 nanosec pulse separation.

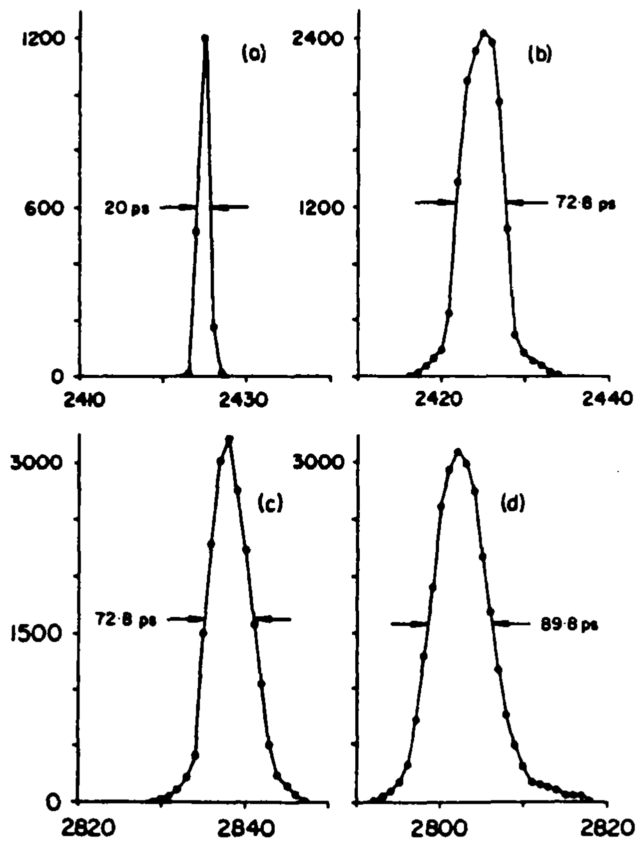

Figure 1 Time spectra obtained during operation of the super buncher. (a) Electronics alone. (b) Electronics plus two detectors. (c) Electronics plus one detector plus bunched beam at 5 m. (d) Electronics plus one detector plus bunched beam at 17 m.

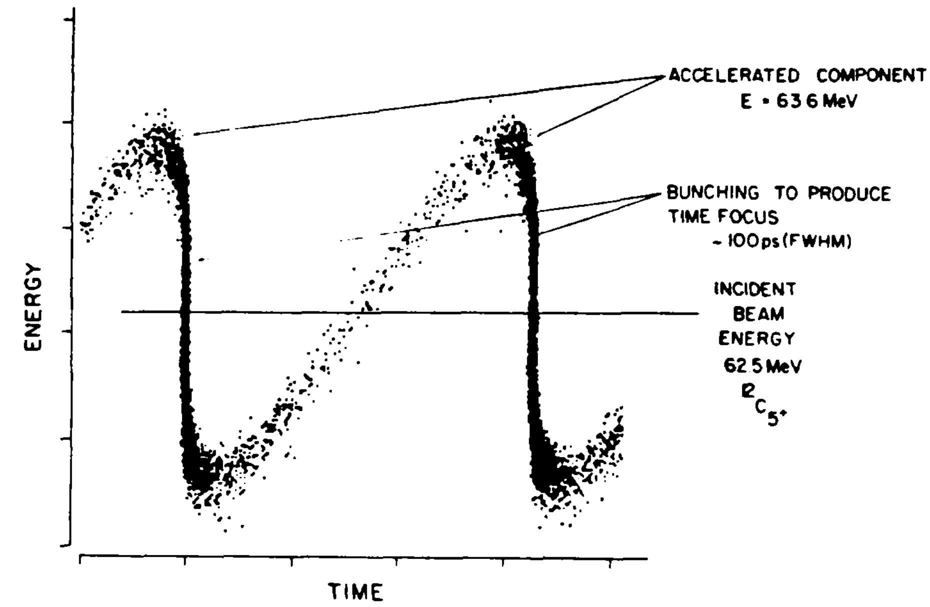

Figure 2 Contour representation of the time distribution versus energy obtained using the super buncher with a d.c. beam.

3.1.2 Chain Breakages and Breakdown Products in SF_6 (Ophel, Cooper and Weisser)

Chain breakage reached crisis point in the review period with six chain breakages occurring during 1982 in addition to frequent detection of cracked nylon links throughout the year.

The last of the chain breaks in late October, after only several hundred hours of operation, led to the decision to suspend operation while the problem was investigated. While some evidence suggested the cause was mechanical (the cracks detected were invariably at the necks of the links and followed machining marks in the nylon), NEC were convinced that severe breakdown product contamination of the SF_6 gas was a significant factor.

A conductivity cell (Figure 1) was developed to detect breakdown products. Follwing earlier work at Oak Ridge, the gas was mixed with boric acid solution and the change of conductivity observed was demonstrated to be correlated with the amount of hydrolyzable fluoride present in the SF_6. Efficient mixing of the gas with the solution was achieved with an atomizer made from teflon.

The atomizer produced a fine mist and was determined to be 100% efficient. The cell response was evaluated with a small corona assembly. This test assembly was also used to determine the characteristics of breakdown product formation by corona and to test the efficacy of removal of the breakdown products by various absorbent materials.

At the start of the investigation period, the gas had an extremely pungent odour but gave a relatively small conductivity cell response. It was found that the alumina being used in the recirculation system was much less effective in removing the breakdown products than new alumina though it had only been in use for six months. Measurements with the conductivity cell of the build up and decay of the breakdown product concentration demonstrated that the recirculation cycle time was 10 hours instead of the nominal 6 hours.

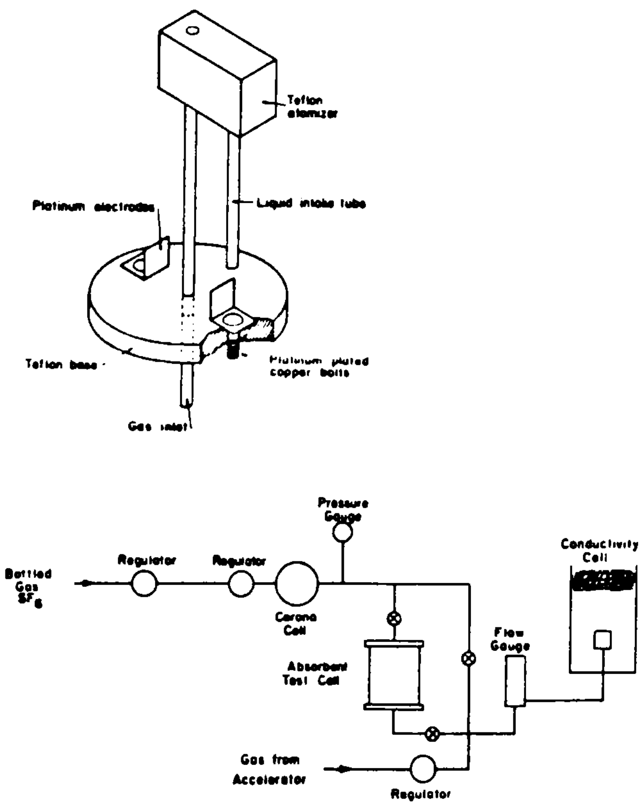

Figure 1 The conductivity cell for monitoring breakdown products in SF_6

As a result of the comparisons of absorbent materials, it was decided to use Vivalyme as well as alumina to purify the gas. Half of the alumina was replaced with Vivalyme so that gas passes firstly through the soda lime for chemical removal of the breakdown products and then into the alumina for drying. The order is important since reactions with Vivalyme produce water.

The accelerator was shut down for six weeks for the investigation and afterwards operation was confined to the use of a single, used chain for a further six weeks to allow monitoring of the gas quality. Two new chains were installed in February 1983. In September, after almost 4000 hours operation, cracks were detected in ~ 10% of the links of one of the chains. The gas quality had been monitored throughout the period, excluding the presence of anomalously large breakdown product concentrations as a contributing cause. A serious oscillation of this chain was found to be occurring (in the "stiff" direction) as a result of pulley misalignment. In this instance at least, we are convinced that the cause of the cracked links was mechanical. A report of the breakdown product measurement techniques will be published shortly.

A testing station has been set up to allow periodic sampling of the gas from three locations; the accelerator tank, the entrance to the purifier and the exit from the purifier. A manifold (Figure 2) makes it possible to flow gas from any of these sources either through the conductivity cell to establish the concentration of breakdown products or to the moisture monitor.

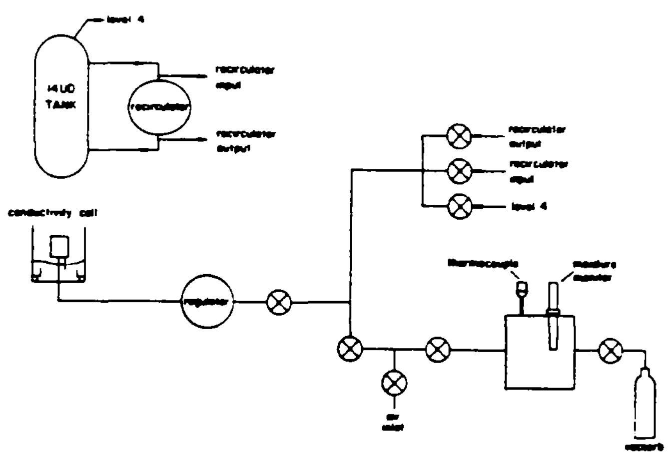

Figure 2 System for monitoring breakdown products and moisture in SF_6 gas

The Shaw Moisture Monitor is housed in a small cell which is evacuated by means of a Vacsorb unit prior to filling with sulphur hexafluoride. The calibration is readily checked by filling the cell with room air. Permanent location of the moisture monitors in the gas handling plumbing proved to be unsatisfactory.

3.2 Fission and Fusion Studies

The three important parameters which enter into statistical evaporation-fission theory are referred to extensively below and are defined here for convenience. They are the level density parameter at equilibrium deformation, a_ν, that at the saddle point deformation, a_f, and the fission barrier B_f. This latter is generally taken to be the Rotating Liquid Drop Model value scaled by a constant k_f.

3.2.1 Multiplicity of pre-fission neutrons (Newton, Charity, Chatterjee, Foote, Hinde, Leigh, Ogaza).

We have previously shown[1] that measurement of the average multiplicity (ν_{pre}) of neutrons preceding fission significantly restricts the large correlated range for the parameters a_f/a_ν and allowed analysis of fusion/fission excitation functions. The ^{200}Pb measurements[1] have been repeated and extended to lower energies, whilst the systems ^{188}Pt, ^{178}W and ^{168}Yb, whose fusion/fission excitation functions have already been reported[2], have also been studied by the same technique at a number of bombarding energies. These systems were investigated through the reactions ^{19}F + ^{169}Tm, ^{19}F + ^{159}Tb and ^{18}O + ^{150}Sm respectively. Preliminary analysis of some of the data gives the results shown in Table 1. Detailed analysis is in progress.

TABLE 1 Multiplicities of pre-fission neutrons

Compound System	Projectile Energy (MeV)	ν_{pre}		a_f/a_ν	k_f
^{200}Pb	95	1.57	)		
	105	2.25	2.02)		
	115	2.30	2.54)	1.02 ± 0.02	0.86(3)
	125		2.69)		
^{188}Pt	105	2.11	)		
	120	2.17	)	1.03 ± 0.02	0.85
			)		
^{178}W	110	2.05		1.02 ± 0.03	0.80
^{168}Yb	108	1.10		1.03 ± 0.05	0.89

References

1) D. Ward et al, Nucl. Phys. A403 (1983) 189.

2) 1982 Annual Report, ANU Dept. of Nucl. Phys.

3.2.2 Neutron Emission from Accelerating Fission Fragments (Hinde, Charity, Chatterjee, Foote, Leigh, Newton, Ogaza)

Following the measurement of pre-fission neutrons (ν_{pre}) for the ^{200}Pb system using the reaction ^{19}F + ^{181}Ta[1], we have studied several other systems, including ^{251}Es (formed by the fusion of ^{19}F with ^{232}Th) using the same experimental apparatus.

Neutron velocity spectra at 0° and 90° to the fission fragment direction were analysed to determine the mean number of neutrons emitted in the rest-frame of the compound nucleus (ν_{iso}), and from the fission fragments (ν_{post}). It is conventionally assumed that all the latter neutrons are evaporated from the fully accelerated fission fragments. With this assumption, the results shown in part (a) of Figure 1 were obtained (where $\nu_{tot} = \nu_{post} + \nu_{iso}$). Surprisingly, ν_{iso} for ^{251}Es is larger than for ^{200}Pb, whereas from fission probability systematics and theory, it should be much smaller (ν_{pre} in the figure). Fission of ^{251}Es produces a gain of 40 MeV in excitation energy, whilst for ^{200}Pb there is approximately no gain. The evaporation of neutrons from the fission fragments is therefore much faster for fission of ^{251}Es, resulting in significant numbers being emitted before the fragments approach their asymptotic velocity (v_∞)[2]. An analysis has been carried out taking this effect into account.

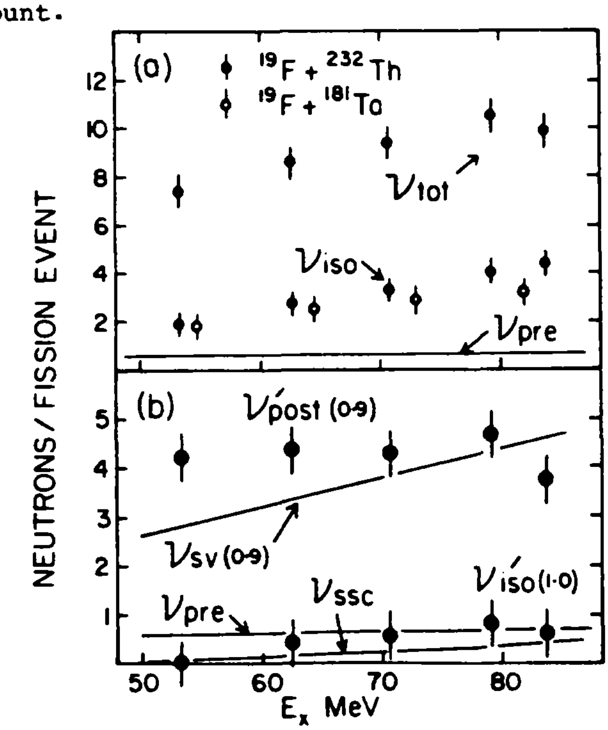

Figure 1 Neutron muliplicities for the ^{251}Es compound system. The results of the conventional analysis in terms of pre- and post-fission neutrons are shown in (a), whilst (b) shows the number of neutrons calculated to be emitted from saddle to scission (ν_{ssc}) and from scission to 0.9 v_∞ ($\nu_{sv}(0.9)$). The points labelled $\nu'_{post}(0.9)$ represent the number of neutrons emitted after 0.9 v_∞.

It was found that, with the level density parameter $a_\nu = A/10$, good agreement between experiment (shown as $\nu'_{iso}(1.0)$ in the figure) and theory (ν_{pre}) could be obtained. Applying these considerations to the ^{200}Pb data, a reduction of ν_{iso} by $\lesssim 0.5$ was obtained.

A similar analysis[3] applied to ^{252}Cf suggested that there is no convincing evidence for scission neutrons. Assuming that this is so, the reduction of ν_{iso} for ^{200}Pb due to neutron evaporation during fragment acceleration is countered by the increase (of ~ 0.4) caused by ignoring scission neutrons. Thus the conclusion that $a_f/a_\nu = 1.02$ is unchanged.

This analysis is being applied to other nuclei studied.

References

1) D. Ward et al, Nucl. Phys. A403 (1983) 189.

2) V.P. Eismont, Sov. J.At.Energy 19 (1965) 1000.

3) K. Skarsvag, Physica Scripta 7 (1973) 160.

3.2.3 Fission Near Mass 200 (Hinde, Charity, Chatterjee, Foote, Leigh, Newton, Ogaza)

We have previously reported measurements of fission and evaporation residue excitation functions for the fusion of ^{18}O with ^{192}Os giving ^{210}Po[1], and ^{16}O with ^{197}Au giving ^{213}Fr[2]. These results have been complemented by recent measurements of pre-fission neutrons. The analysis is still in progress. Together with the earlier measurements, these should allow the parameters a_f/a_ν and k_f to be determined more accurately.

References

1) 1981 Annual Report Department of Nuclear Physics, Section 4.5.

2) 1982 Annual Report Department of Nuclear Physics, Section 5.2.

3.2.4 Neutron Energy Distributions following (HI,xn) Reactions (Leigh, Bokhorst, Chatterjee, Foote, Hinde, Newton, Ogaza)

Our pre-fission neutron multiplicity measurements have been used successfully to limit the ratio a_f/a_ν. The absolute value of a_ν cannot be inferred from multiplicities due to their insensitivity to this parameter[1]. However, the neutron evaporation spectrum is sensitive to a .$_\nu$ Attempts to determine accurately the shape of the pre-fission component were unsatisfactory due to the unavoidable presence of post-fission neutrons. Direct measurements of the spectra of neutrons from compound nuclei have therefore been made using the reactions ^{152}Sm(^{16}O,xnγ)$^{168-x}$Yb and ^{149}Sm(^{18}O,x'nγ)$^{167-x'}$Yb. The bombarding energies were chosen so that the dominant products were the same in the two reactions.

The neutron time-of-flight was measured relative to a beam pulse of ~ 1 nsec FWHM. Pulse shape discrimination was used to identify the neutrons[2]. Coincidences with either of two Compton suppressed Ge detectors were then recorded in event mode. Off line analysis allows the final products to be identified ensuring that only neutrons originating in the compound system decay chain are included. Analysis of the data is in progress. Results will be compared to the predictions of the statistical codes ALERT1 and PACE in order to determine an appropriate level density parameter a_{ν}.

References

1) D. Ward et al, Nucl. Phys. A403 (1983) 189.

2) Link Systems Unit, J.M. Adams and G. White, NIM 156 (1978)459.

3.2.5 Neutron Detector Efficiency Measurement (Hinde, Charity, Leigh, Newton)

The determination of the neutron detector efficiency for the pre-fission neutron measurements previously reported[1] was made using a ^{252}Cf fission source placed in the target position. Neutron velocity spectra at 0°, 45° and 90° to the fission fragment direction were compared with the measurements of Bowman et al[2]. This measurements takes a considerable time, and is subject to some uncertainty. We have developed a technique for measuring the efficiency which does not have these disadvantages.

The ^{252}Cf source is built into a MWPC similar to those reported previously[3], being one of the earth planes. The second earth plane consists of a foil, rather than a grid. This device is located in the target position, and the target chamber is filled with 2 Torr of isobutane. Applying a voltage of +450 V to the central grid results in a pulse for >95% of all fission events from the source.

The neutron velocity spectrum derived using this detector is then divided by the well-known singles neutron spectrum from ^{252}Cf, given to a good approximation by

$$n(v)dv = 0.150\ v^2 \exp(-0.3651\ v^2)\ dv,$$

to give the neutron detector efficiency. This method is over two orders of magniture faster than that used previously. Within the errors of the first measurement, good agreement was obtained between the two methods.

The measured efficiency of a 7.6 x 10.2 cm detector is shown in Figure 1, together with that from a simple calculation[4].

References

1) D. Ward et al, Nucl. Phys. A403 (1983) 189.

2) H.R. Bowman et al, Phy. Rev. 126 (1962) 2120.

3) J.R. Leigh et al, NIM 186 (1981) 541.

4) J.L. Fowler et al, NIM 175 (1980) 449.

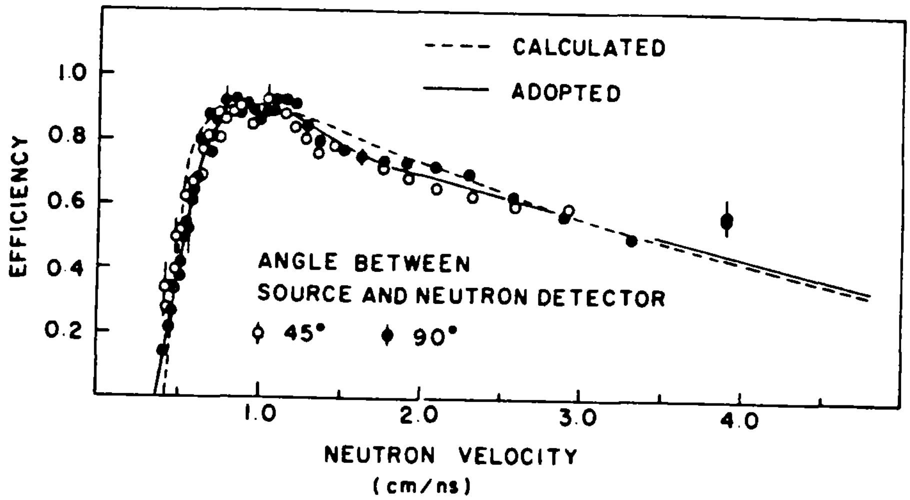

Figure 1

3.2.6 Evaporation from Compound Nuclei with A=100 to 200

(Chatterjee, Charity, Hinde, Foote, Leigh, Newton, Ogaza)

Following a set of experiments aimed at understanding fission and particle evaporation competition for compound systems from A=100 to 200[1], excitation functions for individual evaporation channels were measured.

Using a Compton-suppressed Ge γ-ray spectrometer and two silicon detectors monitoring Rutherford scattering at forward angles, γ-excitation functions for beam energies from 80 to 125 MeV were obtained for the systems

$^{19}F + ^{139}La \rightarrow ^{158}Dy$

$^{18}O + ^{150}Sm \rightarrow ^{168}Yb$

$^{19}F + ^{159}Tb \rightarrow ^{178}W$

$^{19}F + ^{169}Tm \rightarrow ^{188}Pt$

$^{18}O + ^{192}Os \rightarrow ^{210}Po$

For all systems, (xn)-evaporation channels with x = 3 to 8 were identified. A typical example of the excitation functions is shown in Figure 1.

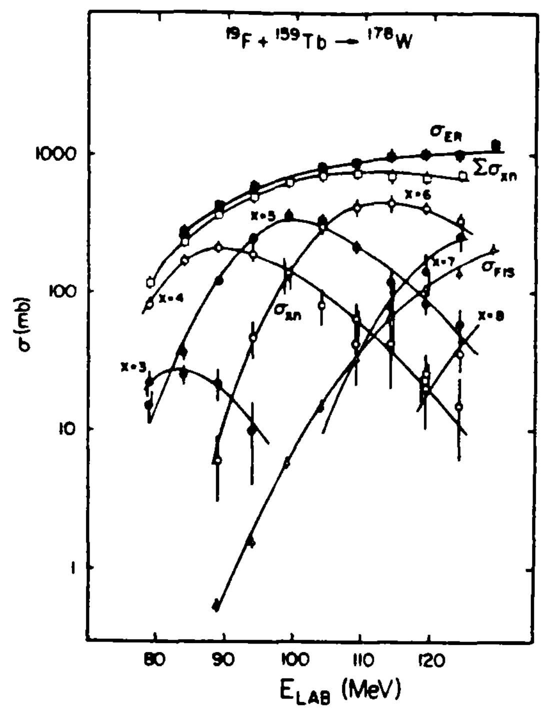

Figure 1 Cross sections for individual exit channels for the ^{19}F + ^{158}Tb reaction

A comparison of the data obtained with theoretical predictions from the evaporation codes ALERT1 and GROGI shows a systematic shift of the experimental excitation functions towards higher energies, resulting in smaller than predicted neutron multiplicity by about 0.5 neutrons. The theoretical estimates are made with a set of parameters which reproduce earlier reported fusion, fission and particle evaporation results[1]. Attempts at understanding the new results by adjusting level density parameters, yrast lines, and γ-emission probabilities are presently being made.

Reference

1) Annual Report, Department of Nuclear Physics, 1982, p.46.

3.2.7 Statistical Model Analysis of Fission and Evaporation Competition in Compound Nuclear Reactions (Charity, Hinde, Leigh, Newton, Foote, Ogaza)

Previous measurements[1] of fission and evaporation residue (ER) excitation functions have been extended for the reactions of ^{19}F on ^{169}Tm, ^{159}Tb, ^{139}La and ^{18}O on ^{150}Sm.

Measurements of both fission and ER cross sections allow the total fusion cross section to be determined ($\sigma_{fus} = \sigma_{fis} + \sigma_{ER}$). These were fitted using the parabolic barrier approximation and compound nuclear angular momentum distributions were extracted.

The fission excitation functions were then analysed with the statistical model computer code ALERT1[2] using the compound nuclear populations extracted from the fusion data. The traditional approach is to fit excitation functions by varying two parameters, a_f/a_ν and k_f. However no parameter sets were found which reproduced the experimental fission excitation functions over the measured energy ranges. At high energies incomplete fusion reactions, which have been observed at higher energies for similar reactions[3], may contribute to the evaporation residue cross section. In view of this, only the lower energy points (E_{lab} < 110 MeV) were fitted. A χ^2 plot obtained for the ^{19}F on ^{159}Tb reaction is illustrated in Figure 1 and is typical of the results found for the other systems. There is no unique solution, but a large range of correlated solutions occupying long valleys in the χ^2 surface. The position of these valleys was found to be sensitive to the initial fusion cross section. Figure 2(b) shows the contours of χ^2 per point increased from the minimum by unity for the three fusion excitation functions shown in Figure 2(a). Each of these excitation functions is consistent with the experimental data.

Large shifts in the valley positions were also observed for different equilibrium level density parameters (Figure 2(b)). Other parameters in the statistical model are expected to produce similar displacements of the χ^2 valleys but to keep the same correlation between a_f/a_ν and k_f. Therefore an independent measurement of a_f/a_ν will greatly restrict the possible values of k_f. Such measurements are in progress (See section 3.2.1).

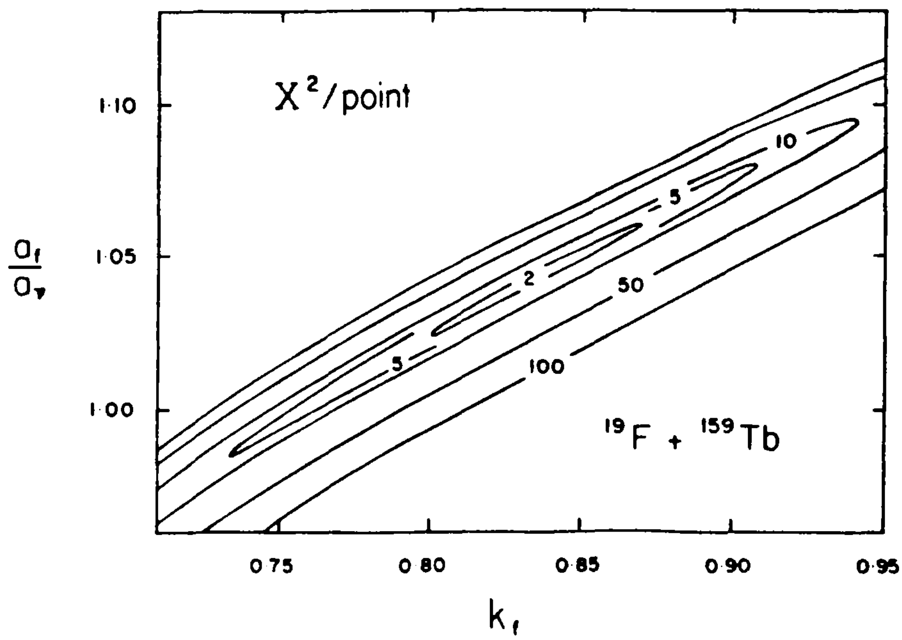

Figure 1 Contour plot of χ^2 per point for statistical model fits to the ^{19}F + ^{159}Tb fission excitation function

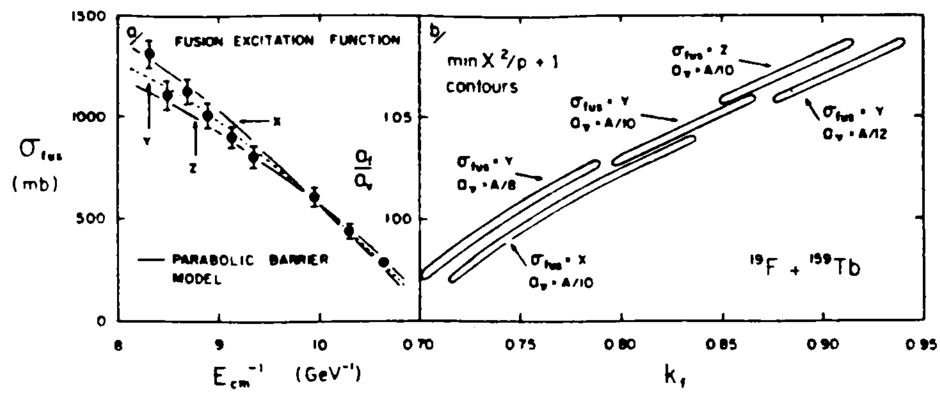

Figure 2 (a) Experimental fusion excitation function for the $^{19}F + ^{159}Tb$ reaction. The three predicted excitation functions obtained from the parabolic barrier approximation cover the range of acceptable fits to these data.

(b) χ^2 per point contours (minimum $\chi^2 + 1$) for the three fusion excitation functions and also for the equilibrium level density parameters, $a_\nu = \frac{A}{8}, \frac{A}{10}, \frac{A}{12}$.

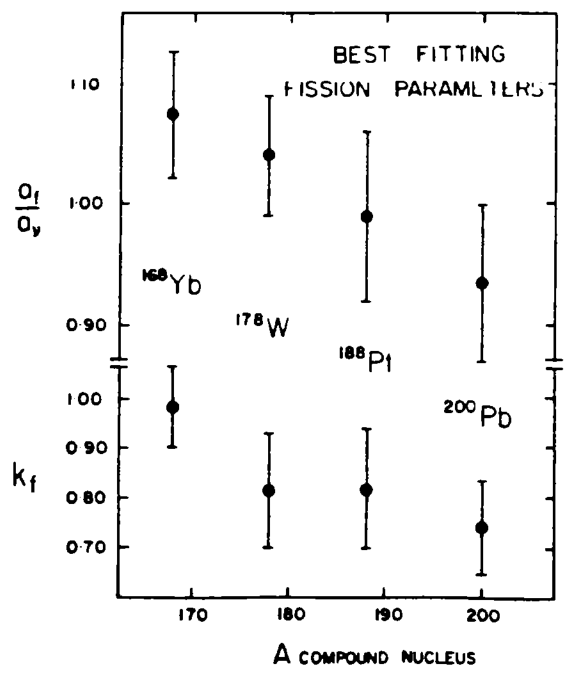

Figure 3 Optimum values of a_f/a_ν and k_f obtained from statistical model fitting as a function of compound nuclear mass.

The best fitting parameter sets are plotted against compound nuclear mass in Figure 3. The data for ^{200}Pb were obtained from previous work[4]. The error on these points contains no components due to other statistical model parameters. The values of a_f/a_ν, and to a lesser extent k_f, show a systematic decrease with increasing mass. As a_f/a_ν is expected to be relatively constant, this systematic behaviour probably results from variation of other statistical model parameters.

References

1) 1982 Annual Report, Department of Nuclear Physics, Section 5.3.

2) M. Blann and T.A. Komoto, Lawrence Livermore National Laboratory Report UCID-19390.

3) J.R. Beene et al, Phys. Rev. C23 (1981) 2463.

4) 1981 Annual Report, Department of Nuclear Physics,Section 4.1.

3.3 Nuclei Far from Stability

3.3.1 The Mass of ^{40}Cl (Fifield, Drumm, Hotchkis, Ophel, Weisser)

As part of a program to measure the masses and level schemes of neutron rich light nuclei, the odd-odd T_z = 3 nucleus ^{40}Cl has been studied using the ^{40}Ar(^{7}Li,^{7}Be)^{40}Cl reaction. The target was argon gas at a pressure of 100 Torr contained within a gas cell (See D3). A spectrum of ^{7}Be ions from the ^{40}Ar(^{7}Li,^{7}Be)^{40}Cl reaction at 54 MeV is shown in Figure 1, together with a spectrum from the ^{14}N(^{7}Li,^{7}Be)^{14}C reaction which was used for calibration purposes. From these spectra the ground state mass excess of ^{40}Cl was determined as -27.527 ± 0.035 MeV. A number of excited states of ^{40}Cl were also observed.

In addition, a measurement of the ^{40}Ar(^{11}B,^{11}C)^{40}Cl reaction was performed in order to resolve possible ambiguities in the identification of peaks in the ^{7}Be spectrum due to excitation of the 0.43 MeV state in ^{7}Be. Simultaneously with the ^{11}C spectrum, a spectrum of ^{13}N ions from the ^{40}Ar(^{11}B,^{13}N)^{38}S reaction was obtained. This spectrum contained peaks corresponding to states in ^{38}S at 1.28 ± 0.04 and 3.38 ± 0.10 MeV. These are presumably the first and second excited states of ^{38}S which have not been reported previously.

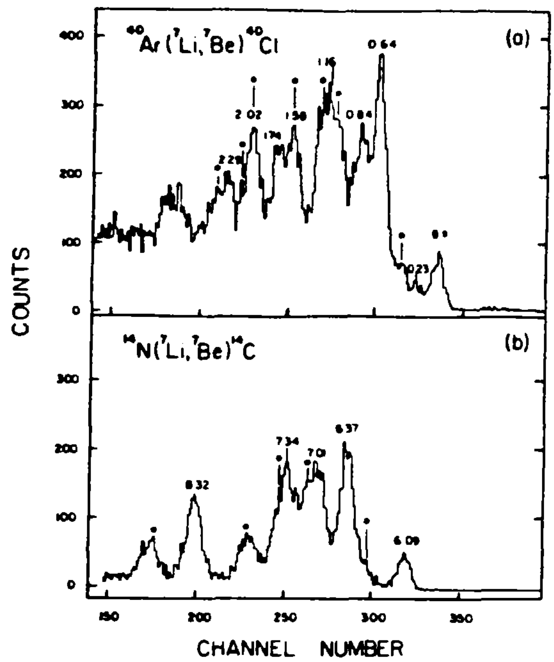

Figure 1 Position spectra of ^{7}Be ions from the ^{40}Ar(^{7}Li,^{7}Be)^{40}Cl and ^{14}N(^{7}Li,^{7}Be)^{14}C reactions at 54 MeV and at a reaction angle of 15°.

3.3.2 The Masses of ^{39}S and ^{41}Cl (Hotchkis, Drumm, Fifield, Ophel, Weisser, Woods)

An ^{18}O beam at 117 MeV was used in conjunction with the gas target to study the ^{40}Ar(^{18}O,^{17}F)^{41}Cl and ^{40}Ar(^{18}O,^{19}Ne)^{39}S reactions. The mass of ^{39}S is unknown, while the mass of ^{41}Cl has been determined previously via a β-decay end-point measurement[1]. Spectra of ^{17}F and ^{19}Ne ions are shown in Figure 2, and lead to values of -27.35 ± 0.10 and -23.07 ± 0.15 MeV for the mass excesses of ^{41}Cl and ^{39}S respectively. These values agree very well with the predictions of the Garvey-Kelson mass equation. The measured mass excess of ^{41}Cl is also in accord with the only previous measurement[1].

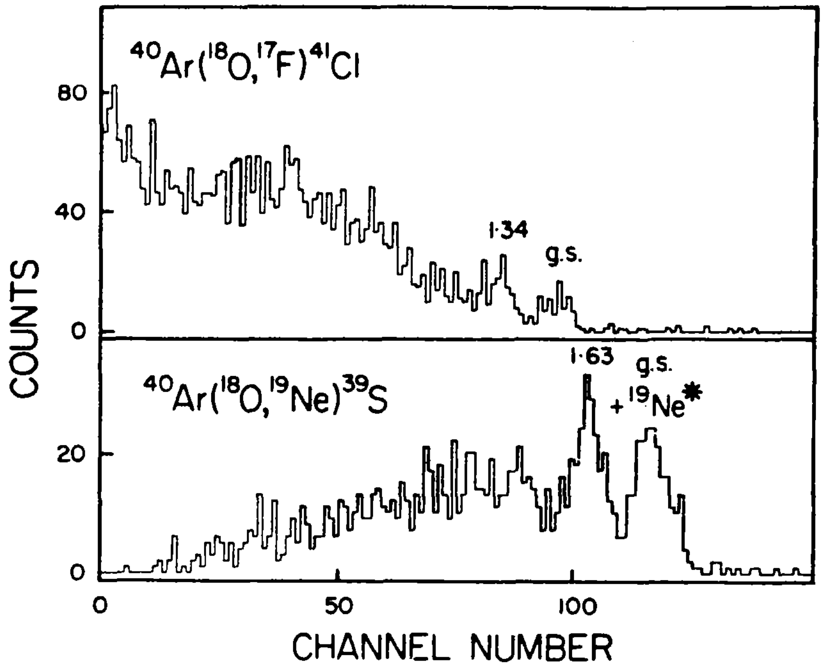

Figure 2   Position spectra of ^{17}F and ^{19}Ne ions from reactions between an ^{18}O beam and an ^{40}Ar target at a reaction angle of 15°.

For ^{39}S, the uncertainty in the mass excess is dominated by the uncertainty in the excitation of the ^{19}Ne ions, the three lowest states of which were not resolved in the present work. A measurement of the $^{40}Ar(^{13}C,^{14}O)^{39}S$ reaction is planned in order to circumvent this problem. A search was also made for ^{18}Ne ions from the $^{40}Ar(^{18}O,^{18}Ne)^{40}S$ reaction. Although ^{18}Ne ions were observed, there were insufficient of them to define a peak corresponding to the ^{40}S ground state.

Reference

1) Kh. Gurach et al, Sov.J.Nucl.Phys. 19 (1974) 596.

3.3.3 Masses and Level Schemes of ^{27}Na and ^{29}Mg (Fifield, Drumm, Hotchkis, Ophel, Weisser, Woods)

The $T_z = 5/2$ nuclei ^{27}Na and ^{29}Mg were produced by the $^{26}Mg(^{18}O,^{17}F)^{27}Na$ and $^{26}Mg(^{18}O,^{15}O)^{29}Mg$ reactions. Spectra taken at a reaction angle of 8° with a beam energy of 110 MeV are shown in Figure 1. These show a number of excited states of both nuclei at excitation energies up to 6 MeV, several of which are observed for the first time. The mass excesses determined from these spectra, -5.52 ± 0.10 MeV for ^{27}Na and -10.64 ± 0.05 MeV for ^{29}Mg are in good agreement with earlier measurements[1,2].

Both reactions have been studied previously by Paschopoulos et al[1] at a beam energy of 82 MeV.

An interesting feature of our results is the very large increase in cross section between 82 and 110 MeV for the $^{26}Mg(^{18}O,^{17}F)^{27}Na$ (g.s) reaction, from 3 to 70 μb/sr. By contrast, the increase in the cross section of the $^{26}Mg(^{18}O,^{15}O)^{29}Mg$(g.s) reaction from 0.7 to 2.7 μb/sr is much more modest.

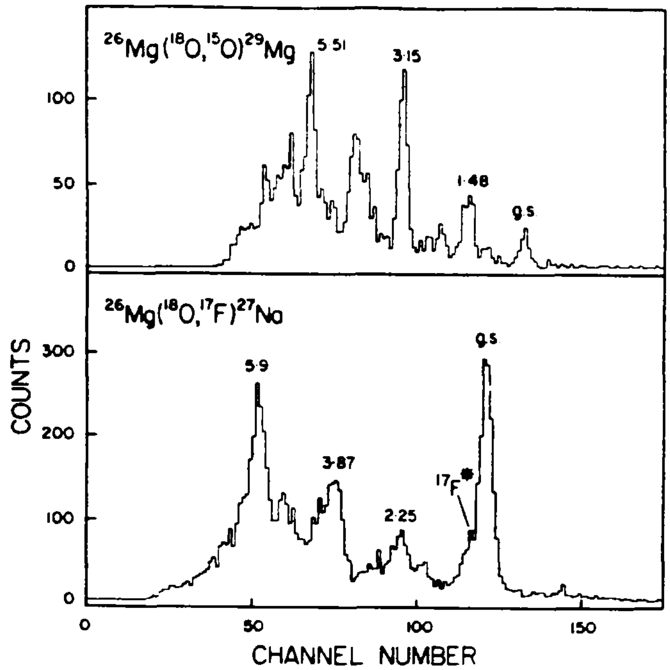

Figure 1 Spectra of ^{15}O and ^{17}F ions from the $^{26}Mg(^{18}O,^{15}O)^{29}Mg$ and ^{26}Mg $(^{18}O,^{17}F)^{27}Na$ reactions at 110 MeV.

A search was also made for ^{14}O ions from the $^{26}Mg(^{18}O,^{14}O)$ ^{30}Mg reaction at the same time. Although ^{14}O ions were present in the data and a clear indication of a wide peak corresponding to a group of excited states of ^{30}Mg was observed, definitive evidence of a peak corresponding to the ^{30}Mg ground state was not forthcoming. In part this was due to a very low cross section (< 50 nb/sr), and in part to background ^{14}O events from reactions on the very small amounts (~ 0.1 μg/cm^2) of ^{24}Mg and ^{40}Ca in the target.

References

1) Paschopoulos et al, Phys. Rev. C18 (1978) 1277.

2) Scott et al, Phys. Rev. Letts. 33 (1974) 1343.

3.3.4 The Mass of ^{21}O (Hotchkis, Drumm, Fifield, Ophel, Weisser)

A precise measurement of the mass of ^{21}O has been made by determining the Q-value of the $^{48}Ca(^{18}O,^{21}O)^{45}Ca$ reaction. An ^{18}O beam energy of 108 MeV was used and reaction products were momentum analysed by the Enge spectrometer.

Ions were identified in the focal plane detector. The mass of ^{21}O was found to be 8.069 ± 0.030 MeV, compared to 8.095 ± 0.075 MeV from the $^{208}Pb(^{18}O,^{21}O)^{205}Pb$ reaction[1] and 8.153 ± 0.070 MeV from the $^{18}O(^{18}O,^{15}O)^{21}O$ reaction[2]. No excited states of ^{21}O were observed in the region studied, which extended up to 2 MeV in excitation. An attempt to identify $^{22}O^{8+}$ ions in this experiment was unsuccessful, due to a large background of inelastic $^{18}O^{7+}$ ions which have similar particle identification signals.

References

1) G.C. Ball et al, Nucl.Phys. A325 (1979) 305.

2) F. Naulin et al, Phys. Rev. C17 (1978) 830.

3.3.5 Search for ^{49}K and $^{51,52}Ca$ (Drumm, Fifield, Hotchkis, Ophel, Weisser).

An attempt was made to measure the unknown masses of ^{49}K and $^{51,52}Ca$ using the $^{48}Ca(^{18}O,^{17}F)^{49}K$ and $^{48}Ca(^{18}O,^{14,15}O)^{51,52}Ca$ reactions. Unfortunately, the calcium targets contained 2.5% of ^{40}Ca, and reactions on this ^{40}Ca gave rise to ^{17}F and $^{14,15}O$ ions of the same rigidity as those from the reactions on ^{48}Ca. Since the reactions on ^{40}Ca have cross sections that are very much larger than those on ^{48}Ca, the spectra were dominated by the ^{40}Ca contribution. As a consequence it was not possible to distinguish any peaks due to reactions on ^{48}Ca.

3.3.6 Search for Low-lying Levels of ^{64}Ge (Fifield, Bark, Drumm, Hotchkis, Woods)

The self conjugate nucleus $^{64}_{32}Ge$ lies in a region of the periodic table where very large deformations might be expected. However, two theoretical models give very different predictions for the excitation energy of its first excited state. A shell model calculation[1] predicts a low-lying level at 300 keV appropriate to a highly deformed nucleus, whereas the SU(4) coloured quark model of Robson predicts this state to lie near 2 MeV, which is not indicative of deformation. Hence a measurement of the energy of the first excited state of ^{64}Ge would be of some interest.

An attempt was made to study the level scheme of ^{64}Ge using the $^{58}Ni(^{16}O,^{10}Be)^{64}Ge$ reaction at an incident energy of 110 MeV with the ^{10}Be ions detected at the focal plane of the Enge spectrometer. The spectrometer was positioned at 5° to the beam direction.

No ^{10}Be ions were observed near the expected position of the ^{64}Ge ground state, and an upper limit of 12 nb/sr has been set on the reaction cross section. To elucidate the reason for this small cross section, that for the precursor α-particle transfer reaction $^{58}Ni(^{16}O,^{12}C)^{62}Zn$ was measured. The value of approximately 20 μb/sr is considerably less than would be required for the $^{58}Ni(^{16}O,^{10}Be)^{64}Ge$ reaction to exhibit a detectable cross section.

References

1) R.K. Sheline, Proc.3rd Int.Conf. on Nuclei far from Stability, Cargese, 1976, CERN 76-12.

2) D. Robson, Nucl.Phys.A308 (1978) 381.

3.3.7 The Role of Odd-Odd Nuclei in Mass Equations (Hotchkis)

Recent experimental studies of light neutron-rich nuclei at this laboratory have prompted an examination of mass formulae used in this mass region. Two methods are widely used:

(i) the Garvey-Kelson (GK) formula[1], which is deduced from mass relationships;

(ii) the modified shell model mass equation (MSMME) of Jelley *et al*[2].

In both cases a large number of parameters are determined from fits to known masses. The GK formula gives a better fit than the MSMME, because it has a proportionately larger number of parameters; but in the sd shell it has been shown[2] that the MSMME leads to more accurate predictions. However, the MSMME suffers from a major drawback: all odd-odd nuclei are excluded because the equation uses an average neutron-proton interaction. This problem can be easily overcome by introducing one more parameter to compensate for the fact that the MSMME consistently overpredicts the masses of odd-odd nuclei by ~ 0.5 MeV. The resulting equation, with a 25% increase in input data at the cost of only one more parameter, actually results in an improved fit to known masses and slightly more accurate predictions in the sd shell than the standard MSMME. Also the wider applicability of the new version can be put to the test if the masses of more $T_z = 3$ odd-odd nuclei are measured.

The reason that this extra paramater is required is due to the nature of the interaction between an unpaired neutron and an unpaired proton in different orbitals. Either a singlet or a triplet interaction is possible, of which the latter is more attractive.

When pairs of neutrons or pairs of protons are involved, there are equal numbers of singlet and triplet interactions, but in the ground state of an odd-odd nucleus (in a simple shell model picture) there will be an extra triplet interaction, resulting in a lower mass than if an average interaction strength is assumed.

References

1) G.T. Garvey *et al*, Rev. Mod. Phys. 41 (1969) S1.

2) N.A. Jelley *et al*, Phys.Rev. C11 (1975) 2049.

3.3.8 The spectroscopy of ^{19}O and the Spin of the ^{18}N Ground State (Sheline)

The spectroscopies of ^{19}O and ^{21}Ne (both 11 neutron systems) are compared in Figure 1. The 3/2+[211↑], 1/2+[220↑] and 1/2-[101↓] bands are observed in both nuclei. On the basis of these similarities ^{19}O is assumed to be a prolate rotor like ^{21}Ne. If the recently studied ^{18}N ground state[1,2]) is also considered to be a deformed system (a proton hole in the ^{19}O nucleus), both the 1- ground state spin and the sudden change in the systematics of the two-neutron binding energies can be understood.

For the 11 neutron system the lowest lying Nilsson orbital is 3/2+[211↑], while for the 7 proton system of this odd-odd ^{18}N nucleus the Nilsson orbital 1/2-[110↓] is predicted. The coupling of these two orbitals, according to the Gallagher-Moskowski coupling rules, energetically strongly favours the triplet or the configuration ν3/2+[211↑]-π1/2-[101↓] to give a 1- ground state as experimentally observed.

A report on this research has been accepted for publication in the Australian Journal of Physics.

References

1) J.W. Olness et al, Nucl. Phys. A373 (1982) 13.
2) G.D. Putt et al, Nucl. Phys. A399 (1983) 190.

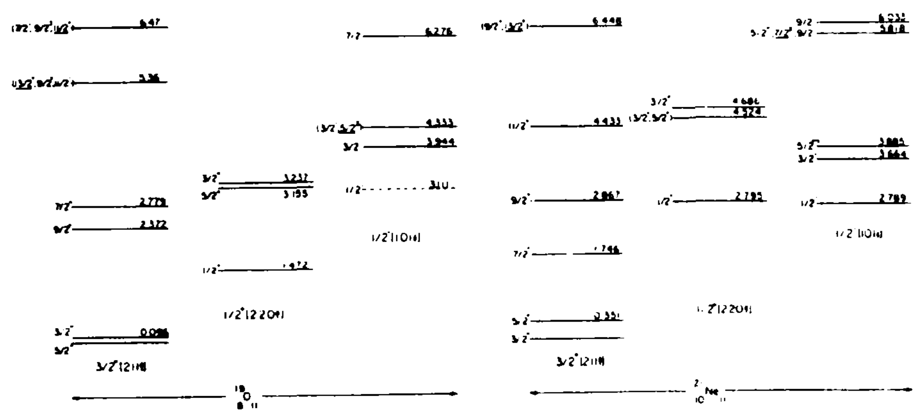

Figure 1 Comparison of rotational band structure in ^{19}O and ^{21}Ne

3.4 Nuclear Reactions and Scattering

In the field of heavy ion resonances, studies of the ^{16}O + ^{24}Mg system have continued with a search for resonant structure in the excitation functions of inelastic scattering to a number of final states in ^{24}Mg. Measurements have also been made of the elastic scattering excitation function at θ_{cm} = 90° in order to define more accurately the positions of the even parity resonances already known to exist in this system. Other systems studied included the mass-30 oxygen plus carbon systems, ^{12}C + ^{18}O and ^{13}C + ^{17}O.

3.5 Coulomb Excitation

Coulomb excitation work has continued with studies of ^{7}Li, ^{208}Pb and the even-mass isotopes of barium. The primary aim of the ^{7}Li work was to measure the effect of the giant dipole resonance on the excitation probability of the 478 keV 1/2- first excited state. The ^{208}Pb measurements were directed towards establishing the static quadrupole moments and reduced transition probabilities of the 2.615(3-) and 4.086(2+) MeV levels. The quadrupole moment of the 3- level was found to be negative and appreciably larger in magnitude than available theoretical predictions. In the even-mass barium isotopes, the B(E3) values for the transitions between the ground state and the 3-octupole vibrational state have been measured for $^{132-138}Ba$.

3.6 Discrete γ-ray Spectroscopy.

One of our visitors initiated a study of the light mercury isotopes, $^{190,192,194}Hg$. The level schemes of all three nuclei have been extended to considerably higher spin than previously known. The three level schemes are similar, and exhibit a second back-bend which may be attributed to the alignment of $h_{11/2}$ protons. Lifetimes of some of the high spin states in ^{190}Hg have been measured by the recoil distance method.

In contrast to the level schemes of the strongly deformed mercury isotopes, the level structures of ^{205}At, ^{209}Rn and $^{211,212,213}Fr$ find an interpretation in terms of the shell model. Each of these nuclei has been investigated up to high spin, and each is characterised by one or more isomeric levels to which specific shell model configurations may be plausibly assigned.

Studies of the realm of excitation energies and angular momenta above the region of the discrete γ-rays have continued with further measurements on heavy-ion fusion reactions and the competition between fission and neutron evaporation in the decay of the compound nucleus. The measurements on the multiplicity of neutrons preceding fission have been extended to systems other than ^{200}Pb, and used to limit the statistical model parameters employed in the analysis of the cross sections. It has been shown that for ^{251}Es an apparently anomalous number of pre-fission neutrons can be explained in terms of neutron emission from fission fragments which have not been fully accelerated. Measurements are also being made of the energy spectra of evaporated neutrons by detecting the neutrons in coincidence with γ-rays from specific residual nuclei. This ensures that neutrons emitted following fission are excluded from the spectra. The pulsed beam was used in this work. These spectra can be used to determine the parameter a_n of the level density at equilibrium deformation.

3.7 Hyperfine interactions

The hyperfine interaction group, largely based in Melbourne but now with a local representative, have continued to exploit the enhanced transient magnetic fields experienced by fast ions in ferromagnets to measure magnetic moments of short lived excited states. Further work to elucidate the origin of this enhanced transient field has also been carried out. Magnetic moments have been measured for low-lying levels in a series of Os isotopes, and for high spin states in ^{158}Er and ^{169}Tm.

3.8 Atomic Collision in Solids

The studies of the charge state distributions of halogen beams emerging from thin carbon foils which were begun last year with bromine beams have been extended to chlorine beams this year. Analysis of the data is directed towards obtaining capture, loss and excitation cross sections for electrons in the various atomic shells. This work is being complemented by measurements of the energy losses of heavy ions in very thin ($\sim$ 2 $\mu g/cm^2$) carbon foils in which the ions do not reach charge state equilibrium.

3.9 Mass Spectroscopy

The metamorphosis of the old $n = 1/2$ double focussing magnetic spectrometer into a high precision mass spectrograph has been completed this year.

After commissioning, considerable effort was expended in understanding mass fractionation effects produced by the ion source, particularly in the three magnesium isotopes. These effects are now believed to be under control, and the spectrometer is being used in the study of isotopic anomalies in Mg and in iron-group elements.

4. AUSTRALIAN RADIATION LABORATORY

4.1 Atomic and Nuclear Data for Transactinide Nuclides (Burns, Johnston and Moroney)

The Radionuclide Metrology Group of the Laboratory has an interest in the determination of accurate emission intensities of α, γ, Kx and Lx radiation of transactinide nuclides. Recent work has involved systematic study of Lx ray emission intensities (Ix) and the parameters which underly them, namely, fluorescence yield (ω_l) and Coster-Kronig transition probabilities (f_{ij}). The methodology adopted is α-gated photon spectrometry with high resolution in both the α and photon channels. Such a system puts severe requirements on the preparation of sources and on the calibration of the photon spectrometer and this has led to the development of new techniques in those areas. The inadequacy of some α-branching ratios was recognised and techniques were developed which gave data with lower uncertainities. The following programs were undertaken:

- the absolute Lx-ray emission rates from ^{230}Th, ^{234}U, ^{237}Np, ^{238}Pu, ^{241}Am and ^{244}Cm were determined with an accuracy for Ix of $1\sigma < 1\%$
- the α-branching ratios of ^{230}Th, ^{234}U, ^{238}Pu and ^{244}Cm were determined by a new method, giving $\alpha^{2+}/\alpha 0$ to $1\alpha << 1\%$
- a preliminary determination was made of ω_2 and f_{23} for $_{88}$Ra, $_{90}$Th, $_{91}$Pa, $_{92}$U, $_{93}$Np and $_{94}$Pu
- the photon spectrometer was calibrated by a new method using coincidence gated determinations in combination with Monte Carlo calculations; spectrometer efficiency from 6 to 25 keV is given to an accuracy of $1\sigma < 1\%$
- the ratio $I_{K\beta}/I_{K\alpha}$ was determined to $1\sigma < 1\%$ for eight elements from Fe to In for use in the calibration of the photon spectrometer
- methods were developed for preparation of sources, for all of the radionuclides of interest, by electrodeposition onto a geometrically-stable substrate, essentially transparent to low-energy photons and suitable for the coincident high-resolution spectrometry in both α and photon channels.

This material is now being prepared for publication.

5. UNIVERSITY OF MELBOURNE

5.1 Photoneutron Cross Section for ^{12}C, ^{14}N and ^{16}O (Facci, Thompson)

The ^{14}N photoneutron cross sections of Berman et al.[1] and King et al.[2] (normalized to join on to the more recent higher energy data of Jury et al.[3] show a significant discrepancy. These cross sections are measured by different methods but should yield the same results below 14.11 MeV. The integrated cross sections up to 14.11 MeV for the preceding cross sections, however, are 3.3 ± o.3 and 0.737 ± 0.009 MeV - mb respectively.

Our work has resolved this difference and to further this work it is intended to relate the integrated photoneutron cross sections up to a certain energy for the 3 light nuclei ^{12}C, ^{14}N, and ^{16}O. The cross sections for these 3 nuclei all display certain discrepancies.

References

1) Berman et al., Phys.Rev. C2, 2318 (1970).

2) King et al., Can.J.Phys. 38, 231 (1960).

3) Jury et al., Nucl.Phys. A337, 503 (1980).

5.2 The $^{17}O(\gamma,n)$ Cross Section (Zubanov, Thompson, Berman**, Pywell+, Jury^{xx}, and McNeill°)

Results of a measurement of the $^{17}O(\gamma,p)$ reaction made using quasimonoenergetic photons from annihilation of positions in flight will be presented.

The reaction yield was determined from the 6.13 MeV gamma rays following from the 7.13 second half-life beta decay of the residual ^{16}N. Using large (11" x 5½" and 8" x 8") NaI detectors. These were placed either side of the sample position so that induced activity could be detected from the sample between beam bursts.

The sample consisted of 3.06 mole of ^{17}O in the form of water. This sample was contaminated with 1.74 mole of ^{18}O, and since the $^{18}O(\gamma,np)$ reaction also leads to ^{16}N, it was necessary to measure this contaminant reaction using a separate ^{18}O-water sample. This separate experiment in fact provides the first measurement of the $^{18}O(\gamma,np)$ cross section.

At each annihilation photon energy, a spectrum was recorded from each detector. From these spectra, the total 6.13 MeV response, per unit photon dose was determined and plotted as a function of incident photon energy after background correction dose normalization and correction for the beamsstrahlung contribution.

**Lawrence Livermore National Laboratory, California, U.S.A.;
+Uni of Saskatchewan; ^{xx}Trent University; °Toronto University.

The most notable and unexpected feature of the cross section is the very large and narrow peak at about 15 MeV, only 1.2 MeV above the reaction threshold. Interpretation of this feature is not clear, but it is probably one or a few T=3/2 states in ^{17}O isospin-forbidden to decay to low-lying states in ^{16}O by neutron emission.

Closer examination shows a general correlation between the features seem in this cross section and that of the photoneutron reaction. However there are significant differences in the relative strengths of some of the peaks. The peak of the GDR as revealed in the photoproton cross section is at 22 MeV, while in the neutron decay cross section it appears at 23 MeV. The ratio of photoproton to photoneutron cross sections depends on isospin considerations.

5.3 Photoneutron Reaction Cross Sections of ^{121}Sb, ^{123}Sb and Nat.Sb (Rassool and Thompson)

The reaction cross sections of $^{121}Sb(\gamma,n)$, $^{123}Sb(\gamma,xn)$ and Nat. $Sb(\gamma,xn)$ have been measured in the energy range 8 to 24 MeV. The ^{121}Sb measurement was obtained by activation using bremsstrahlung. The ^{123}Sb and the Nat. Sb photoneutron reaction cross sections were obtained by directly counting neutrons as a function of bremsstrahlung tip energy. Results are consistent with the predictions of collective models for oblate (negatively) deformed nuclei. Applicability of the Hydrodynamic collective model as describing the observed structure and broadening of the Giant Dipole resonance has been discussed. A comparison has also been made with the Dynamic collective model predictions for oblate nuclei.

5.4 The $^{48}Ca(\gamma,n+p)$ Photonuclear Cross Section in the Giant Dipole Resonance Region (O'Keefe, Assafiri, Thompson)

The $^{48}Ca(\gamma,n+p)$ cross section has been measured from neutron threshold to 25.0 MeV using the activation technique spanning the Giant Dipole Resonance (GDR) region. A measurement of the $^{48}Ca(\gamma,p)$ cross section is used to obtain the $^{48}Ca(\gamma,2n)$ cross section is estimated from a statistical calculation. An estimate to the total photoabsorption for this energy range is then made. The results can be considered in terms of the statistical decay of the GDR with the inclusion of isospin effects according to the predictions of Goulard and Fallieros.

Figure 1 Cross section data between 11 and 25 MeV

5.5 Proton Induced Reactions on ^{37}Cl and their relevance to their relevance to Nucleosynthesis (Webber, Mitchell, Sevior, Tingwell, and Sargood)

The reactions $^{37}Cl(p,\gamma)^{38}Ar$, $^{37}Cl(p,\alpha)^{34}S$, and $^{37}Cl(p,\alpha)^{34}S$ or their inverses, feature in the mainstream of nucleosynthesis in hydrostatic silicon burning and explosive oxygen burning in massive stars. Measurement of their cross section are thereformed astrophysically interesting.

Because the $^{37}Cl(p,n)$ threshold occurs at a low bombarding energy, namely 1.60 MeV (c.m), this set of reactions provides an excellent medium for the study of competion effects between different channels in the context of the statistical model of nuclear reactions.

For both these reasons the cross sections of these reactions have been measured and the data obtained bombarding energies from 0.59 to 2.07 MeV for the (p,γ) and $(p,\alpha\gamma)$ reactions and from threshold to 2.42 MeV for the (p,n) reaction. In all cases the data can be compared with the predictions of the stastistal model code HAUSER*4[1]. Agreement is good for the $(p,\alpha\gamma)$ data but the code overestimates the (p,γ) and (p,n) data by factors ~ 2.

Thermonuclear reaction rates have been determined from the data for the reactions studied and also for the inverse reactions $^{34}S(\alpha,p)^{3}7Cl$ and $^{37}Ar(n,p)^{37}Cl$ over the temperature range $(1\text{-}10) \times 10^{9}K$. The rates are in very mixed agreement with those currently used in nucleosynthesis calculations[2].

The contribution to the rates of $^{37}Cl(p,\gamma)^{38}Ar$ from protons in the energy range 0.7 - 1.8 MeV has also been calculated and compared with rates calculated from published resonance strength data in this energy range[3]. The agreement is excellent.

References

1) F.M. Mann, Hanford Engineering and Development Lab.Rep. No. HEDL-TME-7680 (1976)

2) S.E. WOosley, W.A. Fowler, J.A. Holmes, and B. Zimmerman, Caltech preprint OAP-422 (1975)

3) P.G. Alderliesten, A.M. Aerts, H.M.J. van Bijlert, and C. van der Leun Nucl.Phys. A220 (1974) 284.

5.6 The $^{41}K(p,\alpha)^{38}Ar$ Cross Section and its significance for Nucleosynthesis (Sevior, Mitchell, Tingwell, and Sargood)

The relative strengths of all the decay channels open to states in ^{42}Ca produced by ^{41}Ca+n are of special interest in the nucleosynthesis of many neutron rich nuclei. The only channel for which detailed experimental data do not exist is the alpha-particle channel. These data are most readily accesible via the reaction $^{41}K(p,\alpha)^{38}Ar$, measurements of the cross section of which have been obtained.

5.7 Alpha Particle induced reactions on ^{42}Ca and the mass 45 Bottleneck (Mitchell, Sevior, Tingwell, and Sargood)

There is a bottleneck in the flow of nucleosynthesis in massive stars at mass 45 caused by the abnormally low binding energies in this mass region. The main flows through the bottleneck are currently believed to follow the reaction chains $^{42}Ca(\alpha,p)^{45}Sc(p,\gamma)^{46}Tri$ and $^{42}Ca(\alpha,\gamma)^{46}Ti$. The cross section for $^{45}Sc(P,\gamma)^{46}Ti$ is well known, but published experimental data on $^{42}Ca(\alpha,p)^{45}Sc$ are sketchy, and on $^{42}Ca(\alpha,\gamma)^{46}Ti$ non-existent. Experimental data on both these reaction have been obtained and a comparison with global statistical model calculations has been made.

5.8 The $^{58}Ni(p,\gamma)^{59}Cu$ Cross Section and its importance for Nucleosynthesis and Statistical Model studies (Tingwell, Mitchell, Sevior and Sargood)

One of the most important reactions in determining the abundances of individual isotopes following freeze out from a state of nuclear statistical equilibrium, in supernovae, is $^{58}Ni(p,\gamma)^{59}Cu$[1]. The cross section of this reaction is therefore of great importance for the theory of nucleosynthesis.

Comparisons of statistical model calculations with experimental data for cross sections of (p,γ) reactions on nuclei with a closed shell of 28 neutrons showed the statistical model results to be consistently high by a factor $\gtrsim 2$[2]. It is therefore interesting to see whether a similar effect occurs for nuclei with a closed shell of 28 protons, i.e. the isotopes of nickel.

Cross section data for $^{58}Ni(p,\gamma)^{59}Cu$ have been obtained and their signifi- cance is discussed from the point of view of nucleosynthesis and in terms of the statistical model. In the course of these measurements 60 previously unreported energy levels in ^{59}Cu were observed and their energies have been determined to within ~ 1 keV.

References

1) D.D. Clayton and S.E. Woosley, Rev.Mod.Phys. 46 (1974) 755.

2) S.R. Kennett, L.W. Mitchell, M.R. Anderson and D.G. Sargood, Nucl.Phys. A363 (1981) 233.

5.9 Location of 3p-3h strength in ^{16}N via the reaction $^{13}C(\alpha,p)^{16}N$ at 118 MeV (Andrews, Spicer, Shute, Officer, Collins, Wastell, Nann*, Devins*, Jones*, Olmer*, Qingli Li*)

Differential cross sections of proton groups corresponding to excited states in ^{16}N were measured in the reaction $^{13}C(\alpha,p)^{16}N$ at 118 MeV. Strongly populated stated at 11.21 MeV and 11.81 MeV have been assigned spins $J^{\pi} = 6^{-}$ and $J^{\pi} = 7^{-}$ respectively. Evidence was obtained for the splitting of the 1p-1h $J^{\pi} = 4^{-}$,T=1 strength in ^{16}N on the basis of DWBA calculations incorporating three nucleon microscopic form factors. The addition of a 3p-3h component of 16% was required to fit the data to the known $J^{\pi} = 4^{-}$ state at 6.168 MeV.

---

* Indiana University.

6. UNIVERSITY OF SYDNEY (Peak, McCusker, Winn, Bakich, Omori and Wearne)

The research program of the Falkiner School of Nuclear Physics at the University of Sydney is concerned mostly with particle and high energy physics. For these studies a well shielded underground laboratory is being constructed. The proposed program includes studies of solar neutrinos and double β decay. However, the low background laboratory can be of considerable value in low energy nuclear physics and measurements of spontaneous fission half-lives will be made for several uranium nuclei.

7. WESTERN AUSTRALIAN INSTITUTE OF TECHNOLOGY

7.1 Cumulative Yields of Stable and Long-Lived Isotopes of Tin in Neutron-Induced Fission (Rosman, De Laeter, Boldeman*, Thode+)

Department of Applied Physics, Western Australian Institute of Technology, South Bentley, 6102 Australia.

The relative cumulative fission yields of the six stable isotopes of tin (^{117}Sn, ^{118}Sn, ^{119}Sn, ^{120}Sn, ^{122}Sn, and ^{124}Sn) and the long-lived isotope ^{126}Sn have been measured in the thermal and epicadmium neutron fission of ^{233}U and ^{235}U, and the epicadmium neutron fission of ^{238}U. Nanogram-sized fission product tin samples were extracted from irradiated uranium samples and analyzed in a solid source mass spectrometer. In each case a smooth curve can be drawn through the yield points of the seven isotopes of tin. Figure 1 shows the relative fission yields for thermal and epicadmium fission of ^{235}U. Similar data for ^{233}U are shown in Figure 2 together with epicadmium data for ^{238}U. This work has been published in Canadian Journal of Physics 61 (1983) 1490. There is, therefore, no evidence of "fine structure" in the $117 \leq A \leq 126$ portion of the symmetric mass region.

7.2 p-Process Nucleosynthesis and the Abundances of the Minor Isotopes of Tin (De Laeter, Rosman, Loss)

The minor isotopes of tin are of importance in deciphering mechanisms of nucleosynthesis. In particular ^{115}Sn is a key nuclide in understanding the relative importance of photodisintegration or radiative capture in p-process production. Unfortunately most of the studies of the isotopic composition of tin have suffered from the presence of ^{115}In isobaric interference, which has prevented the abundance of ^{115}Sn from being accurately determined. Recently Devillers and colleagues have measured the absolute isotopic composition of tin in order to determine the atomic weight. However, interferences at masses 114 and 115 were reported. The isotopic composition of tin has been remeasured with the aim of eliminating these interferences. The results show that the isotopic abundance of ^{115}Sn is significantly lower than the presently accepted value. This supports the photodisintegration model of p-process nucleosynthesis. The high sensitivity of the ion enhancing technique now available for tin will enable a search for isotopic anomalies in meteoritic material to be initiated. This research has been published in the Astrophysical Journal 279 (1984) 814.

---

*AAEC; +McMaster University, Canada

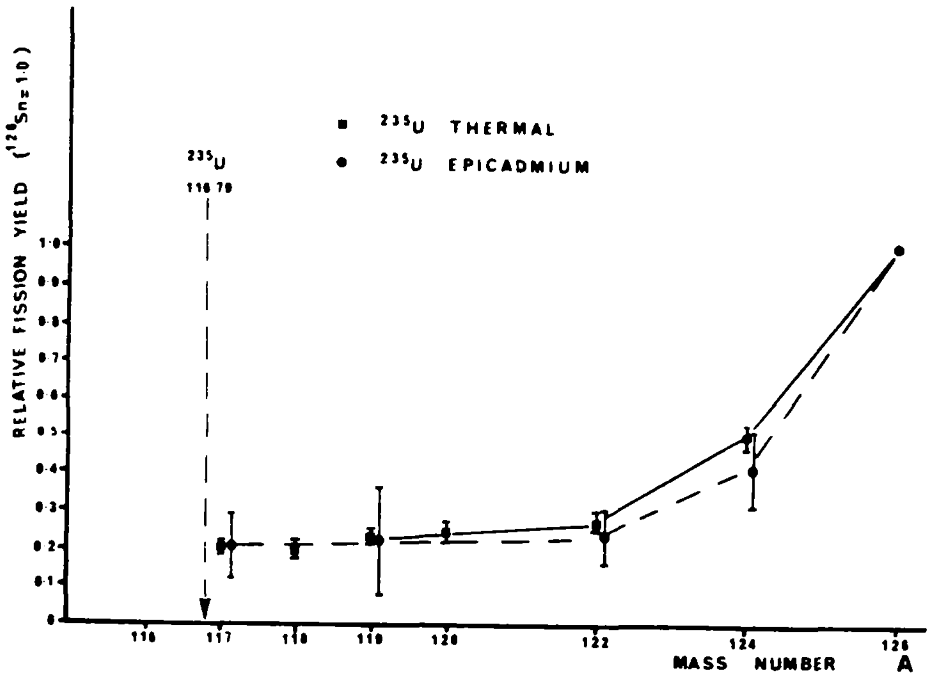

Figure 1 Relative fission yields for tin isotopes for ^{235}U (thermal and epicadmium) normalized to ^{126}Sn.

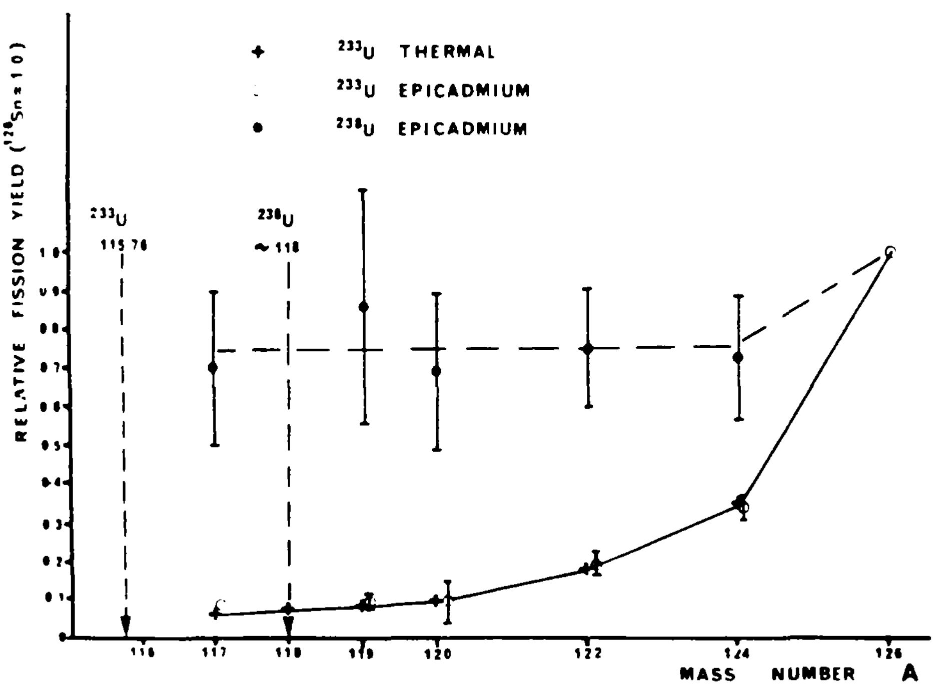

Figure 2 Relative fission yields for tin isotopes for ^{233}U (thermal and epicadmium) and ^{238}U (epicadmium) normalized to ^{126}Sn.

7.3 Transport of Symmetric Mass Region Fission Products at the Oklo Natural Reactors (Loss, Rosman, de Laeter)

The isotopic composition of Pd, Ag, Cd and Te has been measured by solid source mass spectrometry for four samples from reactor zones 2,3-4,5-6 and 7, and from four host rock samples external to the reactor zones from the Oklo mine site. The concentrations of these elements have also been determined in the eight samples using the stable isotope dilution technique. Cumulative fission yields have been derived from the reactor zone samples after correcting where necessary for the terrestrial component of the element concerned.

It has been shown that fission-produced Pd and Te are retained almost in their entirety in the uraninite reactor zone samples, whereas a significant fraction of fission-produced Ag and Cd have migrated from the reactor zones. Fission product Cd is observed in the host rock samples, whereas no strong evidence of fission-produced Ag could be found. Thus the fission-produced Ag which has migrated from the reactor zones has not been retained in the four host rock samples analysed, although the presence of fission product Ag may be masked by the presence of natural Ag. It is possible that the fission product Ag has been retained in the Oklo mine-site, and further host rock samples will be studied to evaluate this possibility. The implications of these results to the storage of radioactive wastes in natural geological repositories is discussed.

This work has been published in Earth and Planetary Science Letters 68 (1984) 240.